Measurable Metrics of Mesenchymal Stem Cell Aging

DOI: 10.17691/stm2025.17.5.01 Received April 22, 2025



D.A. Kalashnikova, Junior Researcher, Laboratory of Epigenetics¹; Junior Researcher, Laboratory of Genomics²;

S.E. Romanov, PhD, Researcher, Laboratory of Epigenetics¹; Researcher, Laboratory of Genomics²;

D.A. Maksimov, PhD, Senior Researcher, Laboratory of Epigenetics¹; Researcher, Laboratory of Genomics²;

I.A. Plokhikh. Junior Researcher. Laboratory of Applied Digital Technologies¹:

R.Yu. Epifanov. Junior Researcher. Laboratory of Applied Digital Technologies¹:

R.I. Mullyadjanov, DSc, Head of the Laboratory of Applied Digital Technologies¹;

Head of the Laboratory of Supercomputing and Artificial Intelligence in Power Engineering³;

L.O. Sidelnikov, Research Assistant, Laboratory of Epigenetics¹;

P.A. Antoshina, Junior Researcher, Laboratory of Genomics²;

Ya.A. Osipov. Research Assistant. Laboratory of Epigenetics1:

V.V. Shloma, PhD, Head of the Laboratory of Genomics²;

A.A. Budilina, Research Assistant, Laboratory of Molecular Mechanisms of Regeneration and Aging⁴;

Junior Researcher, Laboratory of Regenerative Medicine⁵;

E.M. Samoylova, Junior Researcher, Laboratory of Epigenetics¹; Junior Researcher,

Laboratory of Molecular Mechanisms of Regeneration and Aging4;

V.P. Baklaushev, MD, DSc, Head of the Laboratory of Molecular Mechanisms of Regeneration and Aging⁴;

Head of the Laboratory of Regenerative Medicine⁵: Chief of the Center for Biomedical Research⁶:

Head of the Department of Cellular Preparation Development⁷;

P.P. Laktionov, PhD, Senior Researcher, Laboratory of Epigenetics¹; Senior Researcher, Laboratory of Genomics²

¹Novosibirsk National Research State University, 1 Pirogova St., Novosibirsk, 630090, Russia;

²Institute of Molecular and Cellular Biology of the Siberian Branch of the Russian Academy of Sciences. 8/2 Acad. Lavrentiev Avenue, Novosibirsk, 630090, Russia;

³Kutateladze Institute of Thermophysics of the Siberian Branch of the Russian Academy of Sciences,

1 Acad. Lavrentiev Avenue, Novosibirsk, 630090, Russia;

⁴Engelgard Institute of Molecular Biology of the Russian Academy of Sciences, 32 Vavilova St., Moscow, 119991, Russia;

⁵Research Institute of Pulmonology of Federal Medico-Biological Agency of Russia, 28, Bldg. 10, Orekhoviy Blvd., Moscow, 115682, Russia;

⁶Federal Scientific Clinical Center for Specialized Types of Medical Care and Medical Technologies of the Federal Medico-Biological Agency of Russia, 28, Bldg. 1-9, Orekhoviy Blvd., Moscow, 115682, Russia;

⁷Federal Center of Brain Research and Neurotechnologies of the Federal Medico-Biological Agency of Russia,

1, Bldg. 10, Ostrovityanova St., Moscow, 117513, Russia

The aim of the study is to analyze the manifestation of selected cellular senescence markers on the models of replicative senescence, stress-induced senescence, and chronological aging of human mesenchymal stem cells and to study the feasibility of predictive models for assessing the age and duration in vitro cultivation based on the transcriptomic data and investigation of cell morphology.

Materials and Methods. In the study, the dynamics of expression of individual genes encoding key regulators of cellular aging across various models of cellular senescence, as well as telomere length were investigated by real-time PCR. The analysis of the highthroughput transcriptome sequencing datasets of mesenchymal stem cells from the donors of different ages has been performed. Using regression methods, predictive models based on transcriptomic data were developed to estimate chronological age and the duration of

Corresponding author: Petr P. Laktionov, e-mail: laktionov@mcb.nsc.ru

ADVANCED RESEARCHES

in vitro cultivation. Using microscopy methods and subsequent image analysis by machine-learning algorithms, morphological alterations associated with cellular senescence have been explored and segmentation neural network model has been created for extracting nuclear morphology parameters and classification of the cells based on the duration of cultivation in vitro.

Results. CDKN1A, LMNB1, HMGB2 genes demonstrated reproducible similar dynamics on the models of replicative or stress-induced senescence and chronological aging of mesenchymal stem cells. The expression profile of the senescence-associated inflammatory phenotype components was variable in different models of cell aging. The analysis of mesenchymal stem cell transcriptomes from the donors of various ages revealed considerable donor-dependent heterogeneity of the cells, which complicates the development of precise transcriptome data-based predictive models. Investigation of the changes in the telomere length has demonstrated its applicability for assessing the dynamics of replicative senescence in vitro. The developed segmentation neural network model allowed for detecting senescence-associated dynamics of nuclear morphology alterations in the process of replicative aging.

Key words: mesenchymal stem cells; cell senescence; telomeres; expression; predictive models for senescence assessments.

How to cite: Kalashnikova D.A., Romanov S.E., Maksimov D.A., Plokhikh I.A., Epifanov R.Yu., Mullyadjanov R.I., Sidelnikov L.O., Antoshina P.A., Osipov Ya.A., Shloma V.V., Budilina A.A., Samovlova E.M., Baklaushev V.P., Laktionov P.P. Measurable metrics of mesenchymal stem cell aging. Sovremennye tehnologii v medicine 2025; 17(5): 5, https://doi.org/10.17691/stm2025.17.5.01

This is an open access article under the CC BY 4.0 license (https://creativecommons.org/licenses/by/4.0/).

Introduction

Preparations of allogenic and autologous mesenchymal stem cells (MSCs) are considered as a promising component of regenerative cell therapy [1]. In clinical trials, high doses reaching hundreds of millions of cells per one procedure are used. It often requires the expansion of the culture in vitro, which, together with the compromised functional state of the donor's organism, may reduce the quality of cell preparations [2–4]. Functional methods of MSC preparation for clinical application imply the assessment of morphology, cell survival, differentiation potential, and biological safety [5, 6]. At the same time, additional investigations are needed to study the effect of functional state of the donor's organism, cultivation conditions, and duration on the quality of cellular products. When classifying the markers of aging, various functional manifestations such as metabolic and immune disorders, genome instability, and epigenome alterations are distinguished [7]. One of the hallmarks of aging is the accumulation of the senescent cells unable to proliferate, resistant apoptosis, and possessing the characteristic morphological and metabolic phenotype [3, 7].

Inducers of cellular senescence may include the exhaustion of proliferative potential, accompanied by critical telomere shortening; exposure to toxic, genotoxic, and oxidative stress; induction of oncogenes; inflammation; mitochondrial dysfunction; disruption of epigenetic regulatory mechanisms, and other factors [3, 8–11]. It is important to note that the listed factors may also be the secondary effects of cellular aging, and its phenotypic manifestations at the cellular level can vary in a wide range.

Due to its heterogeneity both in vitro and in vivo, there is no specific universal marker of cell senescence [12, 13]. Therefore, the investigation of cellular aging dynamics in general relies on the analysis of several markers, whose combination is inherent to this process [3, 12]. These markers include the induction of senescence-associated β-galactosidase, activation of the cell cycle inhibitors p16INK4A, p21CIP1; reduced expression of LMNB1 and HMGB2 proteins, which shape the structure and architecture of the cell nucleus [14-16]. In addition to the analysis of the mentioned markers, functional tests can be performed to assess proliferative potential, presence of the DNA damage or apoptosis markers [12, 17].

The characteristic feature of the senescent cells is secretion of proinflammatory cytokines, chemokines, growth factors, and proteases, which compose specific senescence-associated secretory phenotype (SASP) [18]. The detection of SASP factors serve as an indicator of cell aging, however, their abundance varies significantly and depends, in particular, on functional cause of the cell senescence [11]. Thus, a classic approach to the exploration of cell senescence is based on the analysis of sufficiently wide spectrum of non-exclusive (non-specific) markers and conducting functional tests. At the same time, the perspective integral assessment of cell senescence by predictive models built on the analysis of DNA methylation patterns, transcriptomic data, and cell morphology is presently being developed [19–21]. These predictive models may consider variability of cell aging phenotype and usually depend, to the lesser extent, on separate markers, which makes them a promising analytical tool.

The aim of the study is to analyze manifestations of selected markers of senescence on the models of replicative senescence, stress-induced senescence, and chronological aging of human mesenchymal stem cells. Among the markers we assessed were the level of expression of individual genes whose expression dynamics are associated with aging, global transcriptome alteration during chronological and in vitro cellular aging; telomere length measurement and changes in cell morphology and manifestations of specific cytological markers of cellular aging. In this study, we evaluated the applicability of these markers for assessment of MSC aging as well as the limitations of methods used that could potentially bias the analysis. In addition, we have analyzed the conceptual feasibility of building predictive models for estimating chronological age and duration of in vitro cultivation based on the transcriptomic data and cell morphology analysis.

Materials and Methods

Cell cultures. Cell samples were obtained from the donors with prior written informed consent. The study was approved by the local ethics committee of the Federal Center of Brain Research and Neurotechnologies of the Federal Medico-Biological Agency of Russia (Protocol No.7-5-22 of September 6, 2022).

In the study, MSCs (n=2) isolated from the Wharton's jelly of the healthy pregnant woman (38-40 weeks of gestation); bone marrow derived MSCs (BM-MSCs) from healthy donors aged 18-25 years (n=3) and donors older than 65 years (n=3) obtained from the mononuclear cell fraction of bone marrow, which was isolated by gradient centrifugation (20 min, 400 g) in the ficoll solution (PanEco, Russia). The cells were cultivated in the DMEM/F12 medium (Servicebio, China) supplemented with 15% fetal bovine serum (Capricorn, Germany) and the antibiotic cocktail of penicillin (100 units/ml) and streptomycin (100 ug/ml) (Gibco. USA). Subculturing was performed at split ratio of 1:4. Using flow cytometry, the expression of the following MSC markers was analyzed: CD29, CD44, CD73, CD90, CD105, CD34, CD45 (FITC/PE; Miltenyi Biotec, Germany), and HLA-DR. The cells exhibited morphology and immunophenotype characteristic of MSCs: CD29+, CD44+, CD73+, CD90+, CD105+, CD34-, CD45-.

For induction of the stress-induced cellular senescence, MSCs were cultured until they reached 60% of confluence, after which the culture medium was replaced with medium containing 200 µM hydrogen peroxide (Dia-m, Russia). After 4 h of incubation, the medium was removed, and MSCs were washed twice with the phosphate-saline buffer. Then the cells were incubated under the standard cultivation conditions for 3 days, after which they were used for further analysis.

Immunostaining and cytochemical analysis of senescence-associated β-galactosidase. Cells were cultured in 96-well plates for confocal microscopy (SPL Lifesciences, South Korea) or on cover glasses precoated with 0.1% gelatin solution (Sigma-Aldrich, USA). Upon reaching the required confluency, the samples were fixed in 4% formaldehyde solution (Sigma-Aldrich, USA). The activity of senescenceassociated β-galactosidase was analyzed using the previously described method [22]. For immunostaining, the cells were incubated in the 0.1% Triton X-100 solution (Amresco, USA) for 30 min, after which they were incubated in 1% BSA solution (Sigma-Aldrich, USA) for 1 h. The following primary and secondary antibodies were used for immunostaining: Ki-67 (Cell

Signalling Technology, USA or Milteny Biotec, Germany); H3K9me3 (Active Motif, USA); Donkey Anti-Mouse IgG H&L (Alexa Fluor® 488) (Abcam, Great Britain); Goat Anti-Rabbit IgG H&L (Alexa Fluor® 568) (Abcam. Great Britain); Goat anti-Rabbit IgG (H+L) (PE-Alexa Fluor™ 647) (Invitrogen, USA). Hoechst 33342 (Invitrogen, USA) was used for nuclear staining. The samples were analyzed using the Olympus BX 51 fluorescence microscope (Olympus Corporation, Japan) and Nikon A1 scanning laser confocal microscope (Nikon Corporation. Japan).

Gene expression analysis using real-time PCR. The Rizol reagent (diaGene, Russia) was used for RNA isolation following the manufacturer's protocol. The complementary DNA was synthesized with reverse transcription reagent kit (Biolabmix, Russia). The realtime PCR was performed using BioMaster UDG HSgPCR SYBR Blue premixes (Biolabmix, Russia). The ACTB and SDHA were used as reference genes for normalization.

Below are the sequences of oligonucleotides used in our work:

ACTB F ACAGAGCCTCGCCTTTG, ACTB RCCTTGCACATGCCGGAG:

SDHA F TTTGATGCAGTGGTGGTAGG, SDHA R CAGAGCAGCATTGATTCCTC;

p21 F TGGAGACTC TCAGGGTCGAAA, p21 R GGCGTTTGGAGTG GTAGAAATC:

HMGB2 F CTTGGCACGATATGCAGCAA, HMGB2 R CAGCCAAAGATAAACAACCATATGA;

LMNB1 F ACACTTCTGAACAGGATCAACC, LMNB1_R CTGTGACACCAGCGTTTGC;

p16ink4a F CCCAACGCACCGAATAGTTA, p16ink4a R ACCAGCGTGTCCAGGAAG:

IL6 F GTGGCTGCAGGACATGACAA, IL6 R TGA GGTGCCCATGCTACATTT;

IL8 F AAGAGCCAGGAAGAACCACC. IL8 R CTGCAGAAATCAGGAAGGCTG;

IL1b F CTGTCCTGCGTGTTGAAAGA, IL1b R TTGGGTAATTTTTGGGATCTACA;

PAI1-F CTCATCAGCCACTGGAAAGGCA, PAI1-R GACTCGTGAAGTCAGCCTGAAAC:

MCP1 F CTTCTGTGCCTGCTGCTCATA, MCP1 R CTTTGGGACACTTGCTGCTG;

MMP1-F TGGACGTTCCCAAAATCCTG, MMP1-R AAGGGATTTGTGCGCATGTAG:

MMP3-F CTGCTGTTGAGAAAGCTCTG, MMP3-R AATTGGTCCCTGTTGTATCCT.

Measurement of the telomere length using real-time PCR. The real-time PCR was performed with BioMaster UDG HS-qPCR SYBR Blue premixes (Biolabmix, Russia) using primer pairs Tel-F CGGTTTGT TTGGGTTTGGGTTTGGGTTTGGGTT and Tel-RGGCTTGCCTTACCCTTACCCTTACCCTTA CCCT specific to telomeric DNA repetitive sequence as well as 36B4u CAGCAAGTGGGAAGGTGTAATCC and 36B4d CCCATTCTATCATCAACGGGTACAA specific to the region of acidic ribosomal phosphoprotein P0 gene on chromosome 12. Genome copy numbers and the total length of the telomeric DNA were determined relative to the DNA strand, represented by the plasmid pAL2-T (Eurogene, Russia) bearing 36B4 genomic region or human telomeric DNA fragment encompassing 14 repetitive units with the total length of 84 bp. The following parameters of amplification were used: 50°C for 5 min, 95°C for 10 min, 39 cycles of 95°C for 15 s and 60°C for 1 min.

Analysis of the next-generation transcriptomic sequencing data and building predictive models based on the transcriptome data. The datasets deposited in the Gene Expression Omnibus repository (GSE139073, GSE145008) were used in our work [23, 24]. Short-read alignment to the reference GRCh38 genome, preprocessing, and detection of gene expression were performed using STAR, SAMtools, and featureCounts programs [25-27]. To eliminate batch effects in the transcriptome data, the ComBat-seq method implemented in the sva package was applied [28]. The statistical edgeR package was employed to analyze the differential gene expression [29].

The predictive models of chronological age and in vitro cultivation duration were created based on the normalized values of gene expression. Genes, whose expression level correlated significantly with the passage or chronological age of the donors, were selected using Spearman and Pearson coefficients of correlation (coefficient >|0.5|, p-value-adjusted <0.05). regressive models were built using LASSO regression and random forest regressor (RFR) from the Scikit-learn package [30]. Data were divided into two sets: the training set (80%, 84 sequencing samples) and the test set (20%, 22 seguencing samples). For the LASSO regressionbased model, automatic tuning of the hyperparameter was applied with LassoCV on the training set. For the RFR model, the base number of tree parameters was used. The model quality was evaluated on the test set which was not involved in the learning process.

Data preparation and training of the neural network segmentation model. In the first stage, using the segment anything image-recognition model followed by manual validation and correction, nuclear masks were generated for microscopic images of cell preparations of umbilical MSCs at different culture passages (passage range — 3-15, a total of 27,500 cells) [31]. At the next stage, images were scaled to the equal resolution and divided by a sliding window with a 246-pixel pitch into the overlapping fragments 256×256 in size. The window step provided an overlap of neighboring image fragments by 10 pixels on each side, which reduced boundary artifacts during the subsequent assembly of the final segmentation map. To increase the model's robustness to various exposure and contrast variations of the images, augmentation methods were employed. Among the transformations used were horizontal and vertical flips, random adjustments of brightness and contrast, as well as scaling with small shifts. The final

dataset comprised 563 examples and was split in an 80 to 20% ratio for training and testing, providing a sufficient number of samples for proper tuning of the network parameters.

For solving the cell nucleus segmentation task, a convolutional neural network architecture, DeepLabV3+ [32] was used. As the backbone network, EfficientNet-b0 [33] pretrained on the ImageNet dataset was selected. providing the models with an initial representation of low-level image features. Training was performed for 40 epochs, allowing the model to reach stable convergence. During this period, the model was trained on a compute node equipped with an NVIDIA A100 GPU, completing the full training cycle in 3.5 h. To minimize the impact of class imbalance (significant differences in nucleus sizes and thin boundaries) and achieve more accurate segmentation, a combined loss function was used, which integrated two components: the BCE-Dice Loss provided high sensitivity to the imbalance between classes (nucleus/background) and accounted for spatial consistency of predictions; the focal loss improved training by reducing the influence of easily classified examples. During training, a learning-rate scheduler was employed, adjusting the learning rate from an initial value of 1e-3 down to 1e-5 after each iteration, ensuring a gradual reduction of the optimization step and promoting stable convergence of the model.

For calculating quantitative morphometric characteristics of nuclei, a binary mask obtained from the DeepLabV3+ segmentation results was passed to the analysis function. Before the calculations, pixels marked as "border" were excluded from the overall mask, after which sequential erosion and dilation (by 20 pixels) were performed to remove thin artifacts and merge broken contours. The parameters computed for each nucleus: center coordinates (X, Y), area, roundness, semi-major/semi-minor axes of the ellipse and inclination angle, the Hausdorff distance. The coefficient of belonging to the class was also established: class 1 (passages 3-5), class 2 (passages 7-9), class 3 (passages 11–15). The executable scripts of the model are deposited in the GitHub repository (https://github. com/LabADTCellSeg/cellseg).

Results

Senescence-associated changes in gene expression profile. To assess the senescenceassociated gene expression dynamics in MSCs we selected genes that might be considered as principle regulators of the cell cycle and nucleus structure, as well as genes encoding components of the proinflammatory phenotype. We examined the expression levels of the following genes — P16INK4a/CDKN2A, P21CIP1/ CDKN1A, LMNB1, HMGB2, IL6, IL8/CXCL8, IL1B, SERPINE1/PAI1, MCP1/CCL2, MMP1, MMP3. Expression analysis was performed on a replicative senescence model: independent umbilical cord MSCs subjected to long-term culture (n=2); on a chronological aging model: BM-MSCs from the donors of different ages: 20-25 years (n=2) and older than 65 years (n=2); on the model of stress-induced cellular senescence: umbilical cord MSCs exposed to hydrogen peroxide to induce cellular senescence (n=2).

The genes encoding cyclin-dependent kinase inhibitors (CDKN2A and CDKN1A) displayed a similar dynamics across all examined samples. Their expression increased during prolonged culture, in response to oxidative stress and with increasing donor age (Figure 1). Notably, the increase of expression was more pronounced for CDKN1A, whereas changes of CDKN2A expression were weaker and, in the context of the replicative aging, insignificant. The expression level of the genes encoding the nuclear architectural proteins LMNB1 and HMGB2 consistently decreased both in replicative and stress-induced senescence models as well as during chronological MSC aging (see Figure 1).

The most dramatic changes were observed during replicative senescence, where the decline in expression over the culture period reached about 90% for both LMNB1 and HMGB2. It is noteworthy that genes encoding the SASP components exhibited different dynamics depending on the cause of cellular senescence (see Figure 1). For example, peroxideinduced senescence led to an increase in the expression levels of all studied genes except MCP1, whereas replicative senescence did not activate the genes encoding matrix metalloproteinases MMP1 and MMP3. It is also worth noting that analysis of the BM-MSCs from the donors of different ages did not reveal age-related changes at the expression levels of the cytokine genes IL-6, IL-1\(\beta\), CXCL8 was weakly activated in the cells of the elderly donors. The SERPINE1/PAI1 gene, encoding PAI-1 protein, appeared to be most stable in the context of aging-associated dynamics of gene expression.

Various manifestations of senescence-associated proinflammatory phenotype depending on the type of cellular senescence are generally expected. Nevertheless, to independently verify the obtained results, we searched for the publicly available highthroughput transcriptome sequencing datasets of cultured MSCs that include donor age and cell passage information in the Gene Expression Omnibus repository. As a result, a dataset (n=37, age 3-85 years, median value 47 years; Table 1) has been prepared and correlation analysis of expression changes in the tested genes with prolonged cultivation and donor age has been performed. According to the obtained results, SERPINE1/PAI1, CDKN1A, and CDKN2A genes demonstrated a positive correlation with culture duration. whereas LMNB1 and HMGB2 showed a negative correlation (Spearman correlation, p<0.05; Table 2). The correlation with the donor age was detected for CDKN1A and LMNB1 genes when no correction for multiple testing was applied (Table 3). Differential expression analysis in BM-MSC samples from donors aged 2035 years (n=7) and donors aged 60-85 years (n=13) has identified only 50 differentially expressed genes (|logFC|>2, p<0.05) (Table 4). It is highly probable that donor-dependent variability of gene expression patterns in MSCs can be quite substantial, making it difficult to identify transcriptional markers of chronological aging. Nevertheless, the expression of individual genes might be applicable for assessing cellular senescence in vitro.

conceptually validate the applicability of transcriptomic data analysis for predicting donors' chronological age or the duration of cell cultivation, we prepared corresponding predictive regression models based on two approaches: LASSO regression and RFR. Genes were selected as predictors based on Pearson and Spearman correlation coefficients, in order to account for both linear and monotonic relationships between features and the target variables chronological age and cultivation duration. As a result, the models based on LASSO regression and RFR have demonstrated close performance: R²=0.755; MAE=9.858 years, and R²=0.742, MAE=10.060 years, respectively (Table 5). The LASSO regression-based model has demonstrated the highest accuracy of the cell passage prediction on the test sample: R²=0.583; MAE=0.508 passages (Table 6).

Analysis of telomere length for cell senescence assessment. One of the traditional markers of assessing cellular aging is the analysis of telomere length. For this analysis we used the real-time PCR method. Samples of umbilical cord MSCs of different passages and BM-MSC samples from the donors aged 20-25 years (n=2) and older than 65 years (n=2) were analyzed on the sixth cultural passage. This method allowed to detect dynamics of the telomere shortening during MSCs cultivation. Statistically significant differences were observed after seven passages (Figure 2). At the same time, when samples from the donors of various ages were compared, no reliable differences were found.

Analysis of nuclear morphology as a marker of cell senescence. To evaluate the dynamics of the nuclear morphology and the expression of individual protein markers during the cell aging, we have analyzed BM-MSC samples of three donors from the young (18-25 years) and older age groups (over 65 years); umbilical cord MSCs exposed to continuous cultivation; and MSCs treated with hydrogen peroxide to induce senescence. In the cytochemical study of senescenceassociated β-galactosidase activity (Figure 3), an increase in its activity was observed during replicative and stress-induced senescence (Figure 3, (b), (c)). When comparing MSCs obtained from the donors of different ages, the differences were not pronounced (Figure 3 (a)).

Immunostaining analysis of the proliferation marker Ki-67 (Figure 4 (a)–(c)) allowed us to detect a relative decrease of the number of Ki-67-positive cells associated with cultivation duration (Figure 4 (a), (d)).

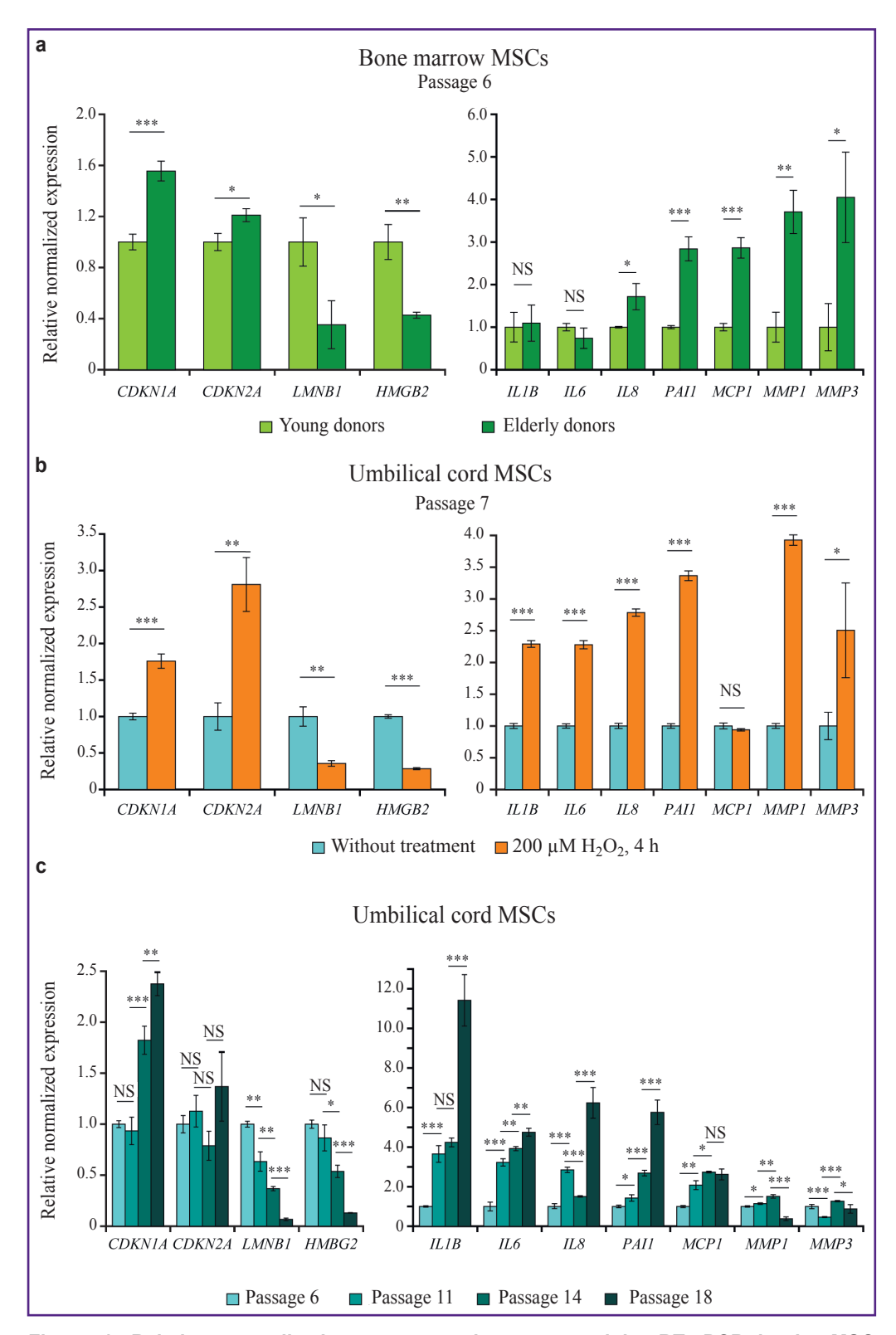


Figure 1. Relative normalized gene expression measured by RT-qPCR in the MSC cultures:

(a) comparison of gene expression in the cultures of MSCs (passage 6) derived from young donors (18-25 years, n=3) and elderly donors (>65 years, n=3); (b) comparison between the umbilical MSCs (passage 7) cultured under standard conditions and after 4-hour treatment of 200 µM solution of hydrogen peroxide; (c) gene expression dynamics during cultivation of umbilical MSCs under standard conditions, measurements taken at passages 6, 11, 14, and 18 are presented; * p<0.05; ** p<0.005; *** p<0.0005; NS — p≥0.05, Student's t-test

Table 1 The list of the RNA-seq datasets used in the study

Sample identifier	Donor age	Gender	Passage	Donor identification number				
Project identifier — GSE139073								
SRR10307337	73	F	4	777				
SRR10307338	73	F	4	777				
SRR10307339	48	F	4	819				
SRR10307340	48	F	4	819				
SRR10307341	75	F	4	821				
SRR10307342	75	F	4	821				
SRR10307343	24	М	3	126				
SRR10307344	24	М	3	126				
SRR10307345	16	F	3	127				
SRR10307346	16	F	3	127				
SRR10307347	61	М	3	237				
SRR10307348	61	М	3	237				
SRR10307349	25	F	3	264				
SRR10307350	25	F	3	264				
SRR10307351	63	М	3	265				
SRR10307352	63	М	3	265				
SRR10307353	48	F	3	276				
SRR10307354	48	F	3	276				
SRR10307355	82	F	3	278				
SRR10307356	82	F	3	278				
SRR10307357	35	F	3	285				
SRR10307358	35	F	3	285				
SRR10307359	45	F	3	289				
SRR10307360	45	F	3	289				
SRR10307361	48	M	3	293				
SRR10307362	48	М	3	293				
SRR10307363	47	F	3	308				
SRR10307364	47	F	3	308				
SRR10307365	71	F	3	316				
SRR10307366	71	F	3	316				
SRR10307367	51	M	3	324				
SRR10307368	51	M	3	324				
SRR10307369	57	M	3	329				
SRR10307370	57	M	3	329				
SRR10307371	80	M	3	336				
SRR10307372	80	M	3	336				
SRR10307373	85	M	3	354				
SRR10307374	85	M	3	354				
SRR10307374	37	M	3	357				
SRR10307376	37	M	3	357				
SRR10307377	68	M	3	374				
SRR10307377 SRR10307378	68	M	3	374				
01610601776	00	IVI	3	3/4				

Continuation of the Table 1

SRR10307379 78 M 3 378 SRR10307380 78 M 3 378 SRR10307381 68 F 3 386 SRR10307382 68 F 3 366 SRR10307383 65 F 3 660 SRR10307384 65 F 3 660 SRR10307385 69 F 3 651 SRR10307386 69 F 3 651 SRR10307388 73 F 3 777 SRR10307389 33 M 3 784 SRR10307390 33 M 3 784 SRR10307391 24 M 6 126 SRR10307392 24 M 6 126 SRR10307393 16 F 6 127 SRR10307394 16 F 6 285 SRR10307395 35 F 6 285	Sample identifier	Donor age	Gender	Passage	Donor identification number
SRR10307381 68 F 3 386 SRR10307382 68 F 3 366 SRR10307383 65 F 3 660 SRR10307384 65 F 3 661 SRR10307385 69 F 3 651 SRR10307387 73 F 3 777 SRR10307388 73 F 3 777 SRR10307399 33 M 3 784 SRR10307390 33 M 3 784 SRR10307391 24 M 6 126 SRR10307392 24 M 6 126 SRR10307393 16 F 6 127 SRR10307394 16 F 6 127 SRR10307395 35 F 6 285 SRR10307397 48 M 6 293 SRR10307398 48 M 6 293 SRR10307400 51 M 6 324 SRR10307401 <td< td=""><td>SRR10307379</td><td>78</td><td>М</td><td>3</td><td></td></td<>	SRR10307379	78	М	3	
SRR10307382 68 F 3 386 SRR10307383 65 F 3 660 SRR10307384 65 F 3 660 SRR10307385 69 F 3 651 SRR10307386 69 F 3 651 SRR10307387 73 F 3 777 SRR10307388 73 F 3 777 SRR10307399 33 M 3 784 SRR10307390 33 M 3 784 SRR10307391 24 M 6 126 SRR10307392 24 M 6 126 SRR10307393 16 F 6 127 SRR10307393 16 F 6 127 SRR10307394 16 F 6 285 SRR10307395 35 F 6 285 SRR10307397 48 M 6 293	SRR10307380	78	М	3	378
SRR10307383 65 F 3 660 SRR10307384 65 F 3 660 SRR10307385 69 F 3 651 SRR10307386 69 F 3 651 SRR10307387 73 F 3 777 SRR10307389 33 M 3 784 SRR10307390 33 M 3 784 SRR10307391 24 M 6 126 SRR10307392 24 M 6 126 SRR10307393 16 F 6 127 SRR10307394 16 F 6 127 SRR10307395 35 F 6 285 SRR10307396 35 F 6 285 SRR10307397 48 M 6 293 SRR10307398 48 M 6 293 SRR10307400 51 M 6 324 SRR10307400 33 M 6 784 SRR1050732	SRR10307381	68	F	3	386
SRR10307384 65 F 3 660 SRR10307385 69 F 3 651 SRR10307386 69 F 3 651 SRR10307387 73 F 3 777 SRR10307388 73 F 3 777 SRR10307390 33 M 3 784 SRR10307391 24 M 6 126 SRR10307392 24 M 6 126 SRR10307393 16 F 6 127 SRR10307394 16 F 6 127 SRR10307396 35 F 6 285 SRR10307396 35 F 6 285 SRR10307397 48 M 6 293 SRR10307399 51 M 6 293 SRR10307400 51 M 6 324 SRR10307402 33 M 6 784 SRR11050732 14 F 3 1 SRR11050733 1	SRR10307382	68	F	3	386
SRR10307385 69 F 3 651 SRR10307386 69 F 3 651 SRR10307387 73 F 3 777 SRR10307388 73 F 3 777 SRR10307390 33 M 3 784 SRR10307391 24 M 6 126 SRR10307392 24 M 6 126 SRR10307393 16 F 6 127 SRR10307394 16 F 6 127 SRR10307395 35 F 6 285 SRR10307396 35 F 6 285 SRR10307397 48 M 6 293 SRR10307400 51 M 6 324 SRR10307400 51 M 6 324 SRR10307401 33 M 6 784 SRR11050732 14 F 3 1	SRR10307383	65	F	3	660
SRR10307386 69 F 3 651 SRR10307387 73 F 3 777 SRR10307388 73 F 3 777 SRR10307389 33 M 3 784 SRR10307390 33 M 3 784 SRR10307391 24 M 6 126 SRR10307392 24 M 6 126 SRR10307393 16 F 6 127 SRR10307394 16 F 6 127 SRR10307395 35 F 6 285 SRR10307396 35 F 6 285 SRR10307399 51 M 6 293 SRR10307400 51 M 6 324 SRR10307401 33 M 6 784 SRR1050732 14 F 3 1 SRR11050733 14 F 3 1	SRR10307384	65	F	3	660
SRR10307387 73 F 3 777 SRR10307388 73 F 3 777 SRR10307389 33 M 3 784 SRR10307390 33 M 3 784 SRR10307391 24 M 6 126 SRR10307392 24 M 6 126 SRR10307393 16 F 6 127 SRR10307394 16 F 6 127 SRR10307395 35 F 6 285 SRR10307396 35 F 6 285 SRR10307398 48 M 6 293 SRR10307399 51 M 6 324 SRR10307400 51 M 6 324 SRR10307401 33 M 6 784 SRR1050732 14 F 3 1 SRR11050733 14 F 3 1	SRR10307385	69	F	3	651
SRR10307388 73 F 3 777 SRR10307390 33 M 3 784 SRR10307391 24 M 6 126 SRR10307392 24 M 6 126 SRR10307393 16 F 6 127 SRR10307394 16 F 6 127 SRR10307395 35 F 6 285 SRR10307396 35 F 6 285 SRR10307397 48 M 6 293 SRR10307398 48 M 6 293 SRR10307400 51 M 6 324 SRR10307401 33 M 6 784 Project identifier — GSE145008 SRR11050732 14 F 3 1 SRR11050733 14 F 3 1 SRR11050734 14 F 3 1 SRR11050735 14	SRR10307386	69	F	3	651
SRR10307389 33 M 3 784 SRR10307390 33 M 3 784 SRR10307391 24 M 6 126 SRR10307392 24 M 6 126 SRR10307393 16 F 6 127 SRR10307394 16 F 6 127 SRR10307395 35 F 6 285 SRR10307396 35 F 6 285 SRR10307397 48 M 6 293 SRR10307398 48 M 6 293 SRR10307400 51 M 6 324 SRR10307401 33 M 6 784 SRR10307402 33 M 6 784 SRR11050732 14 F 3 1 SRR11050733 14 F 3 1 SRR11050734 14 F 3 1 <	SRR10307387	73	F	3	777
SRR10307390 33 M 3 784 SRR10307391 24 M 6 126 SRR10307392 24 M 6 126 SRR10307393 16 F 6 127 SRR10307394 16 F 6 127 SRR10307395 35 F 6 285 SRR10307396 35 F 6 285 SRR10307397 48 M 6 293 SRR10307398 48 M 6 293 SRR10307399 51 M 6 324 SRR10307400 51 M 6 324 SRR10307401 33 M 6 784 SRR10307402 33 M 6 784 SRR1050732 14 F 3 1 SRR11050733 14 F 3 1 SRR11050736 20 M 3 2 <t< td=""><td>SRR10307388</td><td>73</td><td>F</td><td>3</td><td>777</td></t<>	SRR10307388	73	F	3	777
SRR10307391 24 M 6 126 SRR10307392 24 M 6 126 SRR10307393 16 F 6 127 SRR10307394 16 F 6 127 SRR10307395 35 F 6 285 SRR10307396 35 F 6 285 SRR10307397 48 M 6 293 SRR10307398 48 M 6 293 SRR10307399 51 M 6 324 SRR10307400 51 M 6 324 SRR10307401 33 M 6 784 SRR10307402 33 M 6 784 SRR11050732 14 F 3 1 SRR11050733 14 F 3 1 SRR11050734 14 F 3 1 SRR11050735 14 F 3 1 <td< td=""><td>SRR10307389</td><td>33</td><td>М</td><td>3</td><td>784</td></td<>	SRR10307389	33	М	3	784
SRR10307392 24 M 6 126 SRR10307393 16 F 6 127 SRR10307394 16 F 6 127 SRR10307395 35 F 6 285 SRR10307396 35 F 6 285 SRR10307397 48 M 6 293 SRR10307398 48 M 6 293 SRR10307399 51 M 6 324 SRR10307400 51 M 6 324 SRR10307401 33 M 6 784 SRR10307402 33 M 6 784 SRR11050732 14 F 3 1 SRR11050733 14 F 3 1 SRR11050734 14 F 3 1 SRR11050735 14 F 3 1 SRR11050737 20 M 3 2 S	SRR10307390	33	М	3	784
SRR10307393 16 F 6 127 SRR10307394 16 F 6 127 SRR10307395 35 F 6 285 SRR10307396 35 F 6 285 SRR10307397 48 M 6 293 SRR10307398 48 M 6 293 SRR10307399 51 M 6 324 SRR10307400 51 M 6 324 SRR10307401 33 M 6 784 Project identifier — GSE145008 SRR11050732 14 F 3 1 SRR11050733 14 F 3 1 SRR11050734 14 F 3 1 SRR11050735 14 F 3 1 SRR11050736 20 M 3 2 SRR11050737 20 M 3 2 SRR11050738 20 M<	SRR10307391	24	М	6	126
SRR10307394 16 F 6 127 SRR10307395 35 F 6 285 SRR10307396 35 F 6 285 SRR10307397 48 M 6 293 SRR10307398 48 M 6 293 SRR10307399 51 M 6 324 SRR10307400 51 M 6 324 SRR10307401 33 M 6 784 Project identifier — GSE145008 SRR11050732 14 F 3 1 SRR11050733 14 F 3 1 SRR11050734 14 F 3 1 SRR11050735 14 F 3 1 SRR11050736 20 M 3 2 SRR11050737 20 M 3 2 SRR11050740 9 F 3 3 SRR11050741 9	SRR10307392	24	М	6	126
SRR10307395 35 F 6 285 SRR10307396 35 F 6 285 SRR10307397 48 M 6 293 SRR10307398 48 M 6 293 SRR10307399 51 M 6 324 SRR10307400 51 M 6 324 SRR10307401 33 M 6 784 Project identifier — GSE145008 SRR10307402 33 M 6 784 Project identifier — GSE145008 SRR11050732 14 F 3 1 SRR11050733 14 F 3 1 SRR11050734 14 F 3 1 SRR11050735 14 F 3 1 SRR11050736 20 M 3 2 SRR11050737 20 M 3 2 SRR11050740 9 F 3	SRR10307393	16	F	6	127
SRR10307396 35 F 6 285 SRR10307397 48 M 6 293 SRR10307398 48 M 6 293 SRR10307399 51 M 6 324 SRR10307400 51 M 6 324 SRR10307401 33 M 6 784 Project identifier — GSE145008 SRR10307402 33 M 6 784 Project identifier — GSE145008 SRR11050732 14 F 3 1 SRR11050733 14 F 3 1 SRR11050736 14 F 3 1 SRR11050737 20 M 3 2 SRR11050738 20 M 3 2 SRR11050740 9 F 3 3 SRR11050741 9 F 3 3 SRR11050743 9 F 3	SRR10307394	16	F	6	127
SRR10307397 48 M 6 293 SRR10307398 48 M 6 293 SRR10307399 51 M 6 324 SRR10307400 51 M 6 324 SRR10307401 33 M 6 784 Project identifier — GSE145008 SRR10307402 33 M 6 784 Project identifier — GSE145008 SRR11050732 14 F 3 1 SRR11050733 14 F 3 1 SRR11050734 14 F 3 1 SRR11050735 14 F 3 1 SRR11050736 20 M 3 2 SRR11050737 20 M 3 2 SRR11050738 20 M 3 2 SRR11050740 9 F 3 3 SRR11050741 9 F 3	SRR10307395	35	F	6	285
SRR10307398 48 M 6 293 SRR10307399 51 M 6 324 SRR10307400 51 M 6 324 SRR10307401 33 M 6 784 Project identifier — GSE145008 SRR11050732 14 F 3 1 SRR11050733 14 F 3 1 SRR11050734 14 F 3 1 SRR11050735 14 F 3 1 SRR11050736 20 M 3 2 SRR11050737 20 M 3 2 SRR11050738 20 M 3 2 SRR11050740 9 F 3 3 SRR11050740 9 F 3 3 SRR11050741 9 F 3 3 SRR11050742 9 F 3 3 SRR11050744 5 M <td>SRR10307396</td> <td>35</td> <td>F</td> <td>6</td> <td>285</td>	SRR10307396	35	F	6	285
SRR10307399 51 M 6 324 SRR10307400 51 M 6 324 SRR10307401 33 M 6 784 Project identifier — GSE145008 SRR11050732 14 F 3 1 SRR11050733 14 F 3 1 SRR11050734 14 F 3 1 SRR11050735 14 F 3 1 SRR11050736 20 M 3 2 SRR11050737 20 M 3 2 SRR11050738 20 M 3 2 SRR11050740 9 F 3 3 SRR11050740 9 F 3 3 SRR11050741 9 F 3 3 SRR11050742 9 F 3 3 SRR11050744 5 M 3 4 SRR11050746	SRR10307397	48	М	6	293
SRR10307400 51 M 6 324 SRR10307401 33 M 6 784 Project identifier — GSE145008 SRR11050732 14 F 3 1 SRR11050733 14 F 3 1 SRR11050734 14 F 3 1 SRR11050735 14 F 3 1 SRR11050736 20 M 3 2 SRR11050737 20 M 3 2 SRR11050738 20 M 3 2 SRR11050739 20 M 3 2 SRR11050740 9 F 3 3 SRR11050741 9 F 3 3 SRR11050742 9 F 3 3 SRR11050744 5 M 3 4 SRR11050746 9 F 3 5 SRR11050747 9 <t< td=""><td>SRR10307398</td><td>48</td><td>М</td><td>6</td><td>293</td></t<>	SRR10307398	48	М	6	293
SRR10307401 33 M 6 784 SRR10307402 33 M 6 784 Project identifier — GSE145008 SRR11050732 14 F 3 1 SRR11050733 14 F 3 1 SRR11050734 14 F 3 1 SRR11050735 14 F 3 1 SRR11050736 20 M 3 2 SRR11050737 20 M 3 2 SRR11050738 20 M 3 2 SRR11050739 20 M 3 2 SRR11050740 9 F 3 3 SRR11050741 9 F 3 3 SRR11050742 9 F 3 3 SRR11050744 5 M 3 4 SRR11050745 5 M 3 4 SRR11050746	SRR10307399	51	М	6	324
SRR10307402 33 M 6 784 Project identifier — GSE145008 SRR11050732 14 F 3 1 SRR11050733 14 F 3 1 SRR11050734 14 F 3 1 SRR11050735 14 F 3 1 SRR11050736 20 M 3 2 SRR11050737 20 M 3 2 SRR11050738 20 M 3 2 SRR11050739 20 M 3 2 SRR11050740 9 F 3 3 SRR11050741 9 F 3 3 SRR11050742 9 F 3 3 SRR11050744 5 M 3 4 SRR11050745 5 M 3 4 SRR11050746 9 F 3 5 SRR11050748 9 F 3 5 SRR11050749 9 <td< td=""><td>SRR10307400</td><td>51</td><td>М</td><td>6</td><td>324</td></td<>	SRR10307400	51	М	6	324
Project identifier — GSE145008 SRR11050732 14 F 3 1 SRR11050733 14 F 3 1 SRR11050734 14 F 3 1 SRR11050735 14 F 3 1 SRR11050736 20 M 3 2 SRR11050737 20 M 3 2 SRR11050738 20 M 3 2 SRR11050739 20 M 3 2 SRR11050740 9 F 3 3 SRR11050741 9 F 3 3 SRR11050742 9 F 3 3 SRR11050743 9 F 3 3 SRR11050744 5 M 3 4 SRR11050745 5 M 3 4 SRR11050746 9 F 3 5 SRR11050748 9 F 3 5 SRR11050749 9 F 3 5	SRR10307401	33	М	6	784
SRR11050732 14 F 3 1 SRR11050733 14 F 3 1 SRR11050734 14 F 3 1 SRR11050735 14 F 3 1 SRR11050736 20 M 3 2 SRR11050737 20 M 3 2 SRR11050738 20 M 3 2 SRR11050739 20 M 3 2 SRR11050740 9 F 3 3 SRR11050741 9 F 3 3 SRR11050742 9 F 3 3 SRR11050743 9 F 3 3 SRR11050744 5 M 3 4 SRR11050745 5 M 3 4 SRR11050746 9 F 3 5 SRR11050748 9 F 3 5 SRR11050749 9 F 3 5	SRR10307402	33	М	6	784
SRR11050733 14 F 3 1 SRR11050734 14 F 3 1 SRR11050735 14 F 3 1 SRR11050736 20 M 3 2 SRR11050737 20 M 3 2 SRR11050738 20 M 3 2 SRR11050739 20 M 3 2 SRR11050740 9 F 3 3 SRR11050741 9 F 3 3 SRR11050742 9 F 3 3 SRR11050743 9 F 3 3 SRR11050744 5 M 3 4 SRR11050745 5 M 3 4 SRR11050746 9 F 3 5 SRR11050747 9 F 3 5 SRR11050749 9 F 3 5 SRR11050749 9 F 3 5		Project iden	tifier — GSE14	5008	
SRR11050734 14 F 3 1 SRR11050735 14 F 3 1 SRR11050736 20 M 3 2 SRR11050737 20 M 3 2 SRR11050738 20 M 3 2 SRR11050739 20 M 3 2 SRR11050740 9 F 3 3 SRR11050741 9 F 3 3 SRR11050742 9 F 3 3 SRR11050743 9 F 3 3 SRR11050744 5 M 3 4 SRR11050745 5 M 3 4 SRR11050746 9 F 3 5 SRR11050747 9 F 3 5 SRR11050748 9 F 3 5 SRR11050749 9 F 3 5	SRR11050732	14	F	3	1
SRR11050735 14 F 3 1 SRR11050736 20 M 3 2 SRR11050737 20 M 3 2 SRR11050738 20 M 3 2 SRR11050739 20 M 3 2 SRR11050740 9 F 3 3 SRR11050741 9 F 3 3 SRR11050742 9 F 3 3 SRR11050743 9 F 3 3 SRR11050744 5 M 3 4 SRR11050745 5 M 3 4 SRR11050746 9 F 3 5 SRR11050747 9 F 3 5 SRR11050748 9 F 3 5 SRR11050749 9 F 3 5 SRR11050749 9 F 3 5	SRR11050733	14	F	3	1
SRR11050736 20 M 3 2 SRR11050737 20 M 3 2 SRR11050738 20 M 3 2 SRR11050739 20 M 3 2 SRR11050740 9 F 3 3 SRR11050741 9 F 3 3 SRR11050742 9 F 3 3 SRR11050743 9 F 3 3 SRR11050744 5 M 3 4 SRR11050745 5 M 3 4 SRR11050746 9 F 3 5 SRR11050747 9 F 3 5 SRR11050748 9 F 3 5 SRR11050749 9 F 3 5	SRR11050734	14	F	3	1
SRR11050737 20 M 3 2 SRR11050738 20 M 3 2 SRR11050739 20 M 3 2 SRR11050740 9 F 3 3 SRR11050741 9 F 3 3 SRR11050742 9 F 3 3 SRR11050743 9 F 3 3 SRR11050744 5 M 3 4 SRR11050745 5 M 3 4 SRR11050746 9 F 3 5 SRR11050747 9 F 3 5 SRR11050748 9 F 3 5 SRR11050749 9 F 3 5	SRR11050735	14	F	3	1
SRR11050738 20 M 3 2 SRR11050739 20 M 3 2 SRR11050740 9 F 3 3 SRR11050741 9 F 3 3 SRR11050742 9 F 3 3 SRR11050743 9 F 3 3 SRR11050744 5 M 3 4 SRR11050745 5 M 3 4 SRR11050746 9 F 3 5 SRR11050747 9 F 3 5 SRR11050748 9 F 3 5 SRR11050749 9 F 3 5	SRR11050736	20	М	3	2
SRR11050739 20 M 3 2 SRR11050740 9 F 3 3 SRR11050741 9 F 3 3 SRR11050742 9 F 3 3 SRR11050743 9 F 3 3 SRR11050744 5 M 3 4 SRR11050745 5 M 3 4 SRR11050746 9 F 3 5 SRR11050747 9 F 3 5 SRR11050748 9 F 3 5 SRR11050749 9 F 3 5	SRR11050737	20	М	3	2
SRR11050740 9 F 3 3 SRR11050741 9 F 3 3 SRR11050742 9 F 3 3 SRR11050743 9 F 3 3 SRR11050744 5 M 3 4 SRR11050745 5 M 3 4 SRR11050746 9 F 3 5 SRR11050747 9 F 3 5 SRR11050748 9 F 3 5 SRR11050749 9 F 3 5	SRR11050738	20	М	3	2
SRR11050741 9 F 3 3 SRR11050742 9 F 3 3 SRR11050743 9 F 3 3 SRR11050744 5 M 3 4 SRR11050745 5 M 3 4 SRR11050746 9 F 3 5 SRR11050747 9 F 3 5 SRR11050748 9 F 3 5 SRR11050749 9 F 3 5	SRR11050739	20	М	3	2
SRR11050742 9 F 3 3 SRR11050743 9 F 3 3 SRR11050744 5 M 3 4 SRR11050745 5 M 3 4 SRR11050746 9 F 3 5 SRR11050747 9 F 3 5 SRR11050748 9 F 3 5 SRR11050749 9 F 3 5	SRR11050740	9	F	3	3
SRR11050743 9 F 3 3 SRR11050744 5 M 3 4 SRR11050745 5 M 3 4 SRR11050746 9 F 3 5 SRR11050747 9 F 3 5 SRR11050748 9 F 3 5 SRR11050749 9 F 3 5	SRR11050741	9	F	3	3
SRR11050744 5 M 3 4 SRR11050745 5 M 3 4 SRR11050746 9 F 3 5 SRR11050747 9 F 3 5 SRR11050748 9 F 3 5 SRR11050749 9 F 3 5	SRR11050742	9	F	3	3
SRR11050745 5 M 3 4 SRR11050746 9 F 3 5 SRR11050747 9 F 3 5 SRR11050748 9 F 3 5 SRR11050749 9 F 3 5	SRR11050743	9	F	3	3
SRR11050746 9 F 3 5 SRR11050747 9 F 3 5 SRR11050748 9 F 3 5 SRR11050749 9 F 3 5	SRR11050744	5	М	3	4
SRR11050747 9 F 3 5 SRR11050748 9 F 3 5 SRR11050749 9 F 3 5	SRR11050745	5	М	3	4
SRR11050748 9 F 3 5 SRR11050749 9 F 3 5	SRR11050746	9	F	3	5
SRR11050749 9 F 3 5	SRR11050747	9	F	3	5
	SRR11050748	9		3	5
CDD44050750 40 5 0	SRR11050749	9			5
SKK11050/50 13 F 3 6	SRR11050750	13	F	3	6

End of the Table 1

Sample identifier	Donor age	Gender	Passage	Donor identification number
SRR11050751	13	F	3	6
SRR11050752	13	F	3	6
SRR11050753	13	F	3	6
SRR11050754	29	M	3	7
SRR11050755	29	M	3	7
SRR11050756	29	M	3	7
SRR11050757	29	M	3	7
SRR11050758	17	М	3	8
SRR11050759	17	M	3	8
SRR11050760	33	F	3	9
SRR11050761	33	F	3	9
SRR11050762	33	F	3	9
SRR11050763	33	F	3	9
SRR11050764	13	F	3	10
SRR11050765	13	F	3	10
SRR11050766	13	F	3	10
SRR11050767	13	F	3	10
SRR11050768	3	F	3	11
SRR11050769	3	F	3	11
SRR11050770	3	F	3	11
SRR11050771	3	F	3	11

Table 2 Correlation of expression of gene markers of cell senescence with the duration of bone marrow MSC cultivation according to transcriptomic data

Gene	Spearman correlation coefficient	p-value	p-value corrected by the Benjamini–Hochberg method
SERPINE1/PAI1	0.45	1.04E-06	0.000053
HMGB2	-0.33	0.00049	0.0052
LMNB1	-0.31	0.0013	0.011
CDKN1A	0.31	0.0015	0.012
CDKN2A	0.30	0.0017	0.014
CXCL8	0.25	0.011	0.054
CCL2	0.22	0.023	0.090
IL6	0.22	0.024	0.091
IL1B	0.12	0.22	0.44
MMP3	-0.10	0.29	0.53

Table 3 Correlation of expression of gene markers of cell senescence with the age of bone marrow MSCs donors according to transcriptomic data

Gene	Spearman correlation coefficient	p-value	p-value corrected by the Benjamini–Hochberg method
CDKN1A	0.21	0.027	0.14

Gene	Spearman correlation coefficient	p-value	p-value corrected by the Benjamini–Hochberg method
LMNB1	-0.21	0.032	0.16
HMGB2	-0.19	0.050	0.21
MMP3	0.17	0.078	0.27
CXCL8	0.17	0.086	0.28
SERPINE1/PAI1	0.11	0.27	0.53
CCL2	0.10	0.29	0.54
IL6	0.045	0.65	0.82
IL1B	-0.024	0.80	0.91
CDKN2A	-0.014	0.89	0.95

Table 4 Differentially expressed genes in bone marrow MSC RNA-seq samples from donors aged 20-35 years and donors aged 60-85 years

Gene	logFC	logCPM	LR	p-value	FDR
IDO1	-6.74201	0.130015	17.82139	2.43E-05	0.010439
IGKC	-6.03135	1.491429	33.98931	5.54E-09	4.51E-05
CSF3	-6.00031	-0.9205	13.5434	0.00023311	0.038058
CXCL9	-5.91117	-0.96128	13.78282	0.000205204	0.035238
IGHG1	-5.75566	-0.59634	36.87759	1.26E-09	2.66E-05
IGLC2	-5.718	-1.29152	36.70287	1.38E-09	2.66E-05
EEF1DP5	-5.41503	-0.55565	13.93917	0.000188822	0.034148
IGHA1	-5.19498	-1.61628	29.47482	5.66E-08	0.000181
IGKV4-1	-4.98465	-1.7487	30.30424	3.69E-08	0.000151
MYOD1	-4.95005	-1.06079	20.98677	4.62E-06	0.004005
MUC5AC	-4.60036	-1.35788	14.91265	0.000112605	0.02448
IGHG3	-4.53654	-1.75797	22.59954	2.00E-06	0.002714
IGLC3	-4.45419	-1.9868	20.78149	5.15E-06	0.004046
IGHG2	-4.45175	-1.99772	21.74035	3.12E-06	0.003496
GBX2	-4.38756	-1.50842	27.1453	1.89E-07	0.000514
IGLV3-19	-4.23956	-2.06218	20.88334	4.88E-06	0.004005
IGLV3-21	-4.16984	-2.11667	21.59141	3.37E-06	0.003535
IGLV2-14	-3.91505	-2.21161	19.31244	1.11E-05	0.006177
IGHM	-3.60855	-1.94161	13.95801	0.000186939	0.033957
MYOG	-3.60479	-1.94571	13.91752	0.000191009	0.034342
LAIR1	-3.57773	-2.32914	24.23182	8.54E-07	0.001396
TMEM176B	-3.57146	-0.45584	22.1179	2.56E-06	0.003122
ALKAL1	-3.54348	-2.1191	18.05065	2.15E-05	0.00947
IGLV2-11	-3.49343	-2.32861	16.19594	5.71E-05	0.016806
IGKV3-20	-3.40265	-2.3715	15.44576	8.49E-05	0.021421
GCGR	-3.23964	-2.16184	17.18263	3.40E-05	0.01235
IGKV3-15	-3.19646	-2.42303	17.2754	3.23E-05	0.012124
ABO	-3.19078	-1.62966	25.39491	4.67E-07	0.000909
SHD	-3.17845	-1.93949	13.36813	0.000255936	0.039473

Continuation of the Table 4

Gene	logFC	logCPM	LR	p-value	FDR
TNMD	-3.12462	-1.51833	26.04848	3.33E-07	0.000846
MTND1P23	-3.10661	-0.32258	14.56727	0.000135243	0.027729
IGLV2-23	-2.973	-2.26645	12.53699	0.000398975	0.049474
CLDN5	-2.81786	-2.22574	12.53175	0.000400096	0.049474
IGLV6-57	-2.75739	-2.51936	15.10868	0.000101495	0.023174
KRTAP7-1	-2.70262	-2.40336	15.37327	8.82E-05	0.021723
ZFP42	-2.62331	-2.1215	13.22307	0.000276524	0.041179
SCN5A	-2.5801	-1.27536	33.64228	6.62E-09	4.51E-05
NPPB	-2.43186	-1.75835	15.13791	9.99E-05	0.022947
LINC01012	-2.32618	-2.10984	25.94058	3.52E-07	0.000846
KLHL34	-2.29995	-2.32066	13.33429	0.000260597	0.039816
CYP19A1	-2.27558	-2.59913	14.27137	0.000158254	0.031096
CACNA1S	-2.24875	-2.60108	13.49961	0.000238613	0.038058
FAM181B	-2.20795	-1.61487	21.35758	3.81E-06	0.003709
TREML3P	-2.20459	-1.64722	18.8168	1.44E-05	0.007261
SLC51B	-2.08324	-2.08956	20.25594	6.77E-06	0.004944
TRIM72	-2.07456	-2.22947	14.87855	0.000114659	0.024664
HOXC12	-2.02755	0.297099	25.10952	5.42E-07	0.000963
GPX1P2	-2.02304	-2.63327	12.67682	0.000370216	0.048132
LINC03004	-2.00501	-1.67803	13.22407	0.000276377	0.041179
CRTAC1	-1.98816	-1.90343	24.45347	7.61E-07	0.001296
GPR83	-1.95678	-2.02969	19.58557	9.62E-06	0.006084
NKX2-2	-1.95335	-1.98009	15.052	0.000104589	0.023548
PDE1B	-1.93211	-2.01438	13.0485	0.000303527	0.04321
HEY2-AS1	-1.89023	-2.0207	12.65258	0.000375047	0.048415
NOTCH4	-1.88533	-2.50867	12.50129	0.00040667	0.049615
MYH14	-1.88023	0.589392	15.27985	9.27E-05	0.022663
ZNF728	-1.87424	-2.18341	14.43592	0.00014501	0.02877
ZNF99	-1.8592	-2.06605	19.20551	1.17E-05	0.00634
WNK2	-1.80691	-2.04595	16.79481	4.16E-05	0.013727
RSAD2	-1.79102	-1.69653	12.85613	0.000336376	0.046134
DUSP15	-1.73147	-0.94925	22.6271	1.97E-06	0.002714
SUNO1	-1.73101	-1.89769	16.7206	4.33E-05	0.013937
GIPC3	-1.70111	-1.47442	35.46025	2.60E-09	2.66E-05
XIRP1	-1.70079	-0.95231	22.31142	2.32E-06	0.002961
LINC02182	-1.70015	-1.38832	32.94003	9.50E-09	4.86E-05
PCSK1N	-1.69436	-0.279	35.46079	2.60E-09	2.66E-05
RBM12B-DT	-1.68636	-2.31889	13.81687	0.000201519	0.035154
APCDD1	-1.6716	-0.15046	22.09332	2.60E-06	0.003122
TMEM63C	-1.65885	-1.67849	14.07606	0.000175564	0.032973
DUSP26	-1.65032	-1.58372	17.78676	2.47E-05	0.01052
GDF10	-1.6433	-0.98772	16.74222	4.28E-05	0.013937
PHLDA2	-1.6418	0.535531	15.23313	9.50E-05	0.022711
LTK	-1.63865	-1.58262	21.49046	3.56E-06	0.003627

Continuation of the Table 4

Gene	logFC	logCPM	LR	p-value	FDR
LINC00937	-1.59819	-2.06279	19.78999	8.64E-06	0.005791
LHX4	-1.59619	-2.04904	15.95387	6.49E-05	0.017804
TRIM67	-1.59194	-0.12995	13.15763	0.000286351	0.041865
PLXDC1	-1.56106	-1.03286	27.39377	1.66E-07	0.000485
L1CAM	-1.52989	0.276793	14.43591	0.00014501	0.02877
SERPINA12	-1.5203	-0.61139	29.44086	5.76E-08	0.000181
SLC30A3	-1.51219	0.315307	18.86388	1.40E-05	0.007172
FAM162B	-1.50741	-1.53032	15.20718	9.63E-05	0.022759
CMPK2	-1.50377	-1.52247	15.84972	6.86E-05	0.018562
HSPB3	-1.50214	-0.89656	22.53947	2.06E-06	0.002714
TMEM191B	-1.49286	-2.02685	13.79539	0.000203835	0.035154
TMEM156	-1.45208	-1.7143	12.83349	0.00034047	0.046385
TMOD1	-1.43636	-0.74442	21.17288	4.20E-06	0.00393
GPAT2P1	-1.40596	-1.70658	12.56297	0.000393465	0.049474
GPR27	-1.40062	0.30417	19.32474	1.10E-05	0.006177
CDH8	-1.39788	-0.37092	17.14553	3.46E-05	0.01235
CACNA2D3	-1.39769	2.11436	14.7683	0.000121562	0.025479
HEY2	-1.39228	2.025565	19.43099	1.04E-05	0.006177
ST8SIA2	-1.39093	-0.49211	17.53827	2.82E-05	0.010961
LINC02056	-1.38857	-1.62073	12.69264	0.000367098	0.048132
LRP2	-1.37985	-1.28367	23.2891	1.39E-06	0.00211
TGFA	-1.37091	-0.4596	25.61174	4.17E-07	0.000853
WFDC1	-1.36441	2.938302	15.38643	8.76E-05	0.021703
HES4	-1.34238	2.562402	17.64995	2.66E-05	0.010735
PTH1R	-1.33645	0.127042	20.95353	4.71E-06	0.004005
SYN2	-1.26943	1.567083	12.94207	0.000321279	0.044663
HOXC13	-1.26823	-0.37058	19.43103	1.04E-05	0.006177
RAI2	-1.26422	-0.02813	12.60263	0.000385204	0.048893
LONRF2	-1.21634	0.213618	16.65195	4.49E-05	0.014227
HEYL	-1.2162	2.019352	18.99141	1.31E-05	0.00688
CSPG5	-1.21002	-1.72016	18.2359	1.95E-05	0.008993
HEY1	-1.20268	-0.67351	13.30536	0.000264648	0.040107
SLFN14	-1.19595	-1.77817	13.91193	0.000191579	0.034342
ADCY2	-1.1846	2.069172	15.06383	0.000103936	0.023548
RASGRP2	-1.17855	-0.48357	14.0089	0.000181948	0.033347
HOXC13-AS	-1.17836	-1.28119	15.17852	9.78E-05	0.022901
WIPF3	-1.17172	-0.55415	19.45319	1.03E-05	0.006177
PDZD4	-1.16655	0.813909	17.21875	3.33E-05	0.01235
CCDC3	-1.16413	1.018813	15.73623	7.28E-05	0.0192
NPTX1	-1.15928	-1.25645	13.03203	0.000306208	0.04321
CNTN1	-1.15545	0.424462	12.51781	0.000403091	0.049474
ADAP1	-1.1469	-0.05287	25.73178	3.92E-07	0.000853
ITIH5	-1.13921	6.341922	13.5147	0.000236702	0.038058
LINC00547	-1.13275	0.376618	17.9216	2.30E-05	0.010009

Continuation of the Table 4

Gene	logFC	logCPM	LR	p-value	FDR
SOX18	-1.12464	1.243256	15.23793	9.48E-05	0.022711
LGALS9	-1.11907	-0.08648	14.93291	0.000111402	0.024348
LINC01362	-1.07221	-1.14826	16.16752	5.80E-05	0.016806
NAP1L2	-1.06613	-1.41077	18.36179	1.83E-05	0.008698
SLC24A3	-1.06481	3.570396	14.93962	0.000111007	0.024348
KNDC1	-1.04924	-0.4902	12.71091	0.000363528	0.048132
TMEM151A	-1.04248	0.0769	13.21936	0.000277072	0.041179
CX3CL1	-1.0329	-0.55568	19.79463	8.62E-06	0.005791
GNAO1	-1.02459	0.68505	12.50729	0.000405366	0.049604
KCNB1	-1.00315	1.293309	13.64308	0.000221055	0.036797
KL	-0.99468	-1.5026	12.69037	0.000367543	0.048132
CDH15	-0.96785	3.09543	21.71385	3.16E-06	0.003496
FGFR3	-0.96435	1.855654	18.18702	2.00E-05	0.008993
RTN1	-0.95672	-0.85915	13.51578	0.000236566	0.038058
SORBS1	-0.91465	0.58739	12.917	0.000325611	0.045108
GPRC5C	-0.91125	1.346111	17.15483	3.45E-05	0.01235
FOLR1	-0.90256	0.48096	12.62354	0.000380919	0.048707
ADCY1	-0.89133	0.016148	16.82263	4.10E-05	0.013637
CD247	-0.88122	-0.95038	20.89899	4.84E-06	0.004005
PHOSPHO1	-0.87691	-1.10453	19.19722	1.18E-05	0.00634
RNASEK	-0.8769	-1.24948	15.80022	7.04E-05	0.018682
LRRC3	-0.87242	2.006731	17.69325	2.60E-05	0.010735
ACAN	-0.87036	10.49467	19.38983	1.07E-05	0.006177
WDR87BP	-0.86428	0.707841	14.02695	0.000180209	0.033327
AKAP6	-0.85959	2.440635	18.39394	1.80E-05	0.008698
TSPAN15	-0.85178	2.428343	15.81195	7.00E-05	0.018682
CARMIL2	-0.83114	-0.62056	12.58457	0.000388945	0.049215
FAM83H	-0.80075	-0.53574	19.45025	1.03E-05	0.006177
MARK1	-0.79935	1.851002	17.57187	2.77E-05	0.010872
TPD52	-0.79811	0.520582	15.93241	6.56E-05	0.017887
DYSF	-0.79424	5.192088	14.96679	0.00010942	0.0243
FAM169A	-0.77762	-0.93632	13.44043	0.00024626	0.038563
NOG	-0.77472	3.337352	13.13857	0.000289278	0.042065
ADRA1B	-0.77342	-0.31774	12.53894	0.000398558	0.049474
SHANK2	-0.76822	2.303994	13.88607	0.000194233	0.034666
BRSK2	-0.74595	0.213741	13.98842	0.00018394	0.033562
DNAH10	-0.73965	-0.88267	13.19353	0.000280917	0.041599
RYR1	-0.73799	-0.41911	13.08336	0.00029793	0.042876
LEPR	-0.73782	8.314245	13.50392	0.000238066	0.038058
SHC4	-0.73431	1.564619	15.21512	9.59E-05	0.022759
GIPR	-0.73217	0.662796	15.49546	8.27E-05	0.021049
ENPEP	-0.71631	1.032989	14.88719	0.000114135	0.024664
LINC02600	-0.71439	-0.12262	13.67039	0.000217862	0.036643

Continuation of the Table 4

Gene	logFC	logCPM	LR	p-value	FDR
RASL11A	-0.70716	2.188546	14.50159	0.000140041	0.028335
NPTXR	-0.707	5.032025	13.53486	0.000234173	0.038058
TMEM54	-0.69739	0.126718	13.38037	0.000254272	0.039365
FOXCUT	-0.694	0.89011	16.11985	5.95E-05	0.017113
ARHGEF16	-0.68756	1.494923	12.51938	0.000402753	0.049474
FAM89A	-0.68137	3.487588	15.6699	7.54E-05	0.019758
GPAT2	-0.67632	1.848891	14.75442	0.00012246	0.025536
ITGAL	-0.6678	0.188307	15.82416	6.95E-05	0.018682
IGFBP2	-0.66553	8.122881	13.76376	0.000207297	0.035238
CASQ1	-0.65423	-0.07883	13.49412	0.000239312	0.038058
IL7R	-0.64593	4.366858	13.44428	0.000245754	0.038563
SLC16A14	-0.6331	0.173104	13.79726	0.000203632	0.035154
MICA	-0.6268	2.579888	17.04439	3.65E-05	0.012756
GP1BB	-0.614	2.047757	15.41856	8.61E-05	0.021598
DGKG	-0.61299	1.438626	14.59997	0.000132917	0.027437
JPH2	-0.60239	5.92529	13.87562	0.000195316	0.0347
EDN1	-0.59572	2.794714	12.7033	0.00036501	0.048132
CCDC158	-0.5949	1.517501	14.05138	0.000177883	0.033047
ADRA2C	-0.59458	3.684148	12.98359	0.000314233	0.043983
EGFL7	-0.59008	3.282763	14.19471	0.000164834	0.032081
ITGB1BP2	-0.58525	-0.13723	13.22001	0.000276977	0.041179
LYL1	-0.58504	0.516555	12.62508	0.000380605	0.048707
ZSWIM5	-0.5718	0.176161	15.03511	0.000105529	0.023569
QPRT	-0.57054	1.791185	20.97442	4.65E-06	0.004005
СКВ	-0.54894	6.4886	21.15728	4.23E-06	0.00393
SYNGR2	-0.54869	4.063023	17.63299	2.68E-05	0.010735
C3orf70	-0.53617	2.258994	14.40221	0.000147629	0.029148
SEPTIN5	-0.53548	5.850167	17.71423	2.57E-05	0.010735
LGMN	-0.5295	7.390066	13.44756	0.000245325	0.038563
CRIP1	-0.5278	5.915864	15.04709	0.000104862	0.023548
LINC00702	-0.52483	1.68425	18.78584	1.46E-05	0.007289
SLC37A1	-0.51686	2.285977	15.25594	9.39E-05	0.022704
SRRM3	-0.50967	1.020992	12.7151	0.000362716	0.048132
ZNF469	-0.50237	6.320352	21.44639	3.64E-06	0.003627
CRYAB	-0.50215	8.082892	18.24895	1.94E-05	0.008993
DNAJC6	-0.50021	3.746198	16.17961	5.76E-05	0.016806
PPFIA3	-0.49208	1.786657	18.40639	1.78E-05	0.008698
CGREF1	-0.48846	3.916935	15.49059	8.29E-05	0.021049
DNAH5	-0.48696	1.114283	14.10597	0.000172794	0.032848
HES6	-0.48063	1.574922	20.41189	6.24E-06	0.00464
CSPG4	-0.47527	7.532437	13.59239	0.000227104	0.037427
IRAG1	-0.45697	4.251489	12.48452	0.000410338	0.04986
TBXA2R	-0.45102	2.367274	17.31301	3.17E-05	0.011997

Continuation of the Table 4

Gene	logFC	logCPM	LR	p-value	FDR
HS6ST1	-0.44571	5.327054	13.75934	0.000207785	0.035238
DMPK	-0.44482	6.388112	29.74076	4.94E-08	0.000181
LYSMD2	-0.41007	1.900144	13.60586	0.00022548	0.03731
ANKRD9	-0.40992	4.467814	17.67927	2.61E-05	0.010735
NOTCH3	-0.40918	9.646443	15.15878	9.88E-05	0.022945
ISG20	-0.39744	2.672711	13.30319	0.000264954	0.040107
ADORA2B	-0.39485	2.24752	14.86052	0.000115761	0.024756
GPC4	-0.39132	6.164633	16.08634	6.05E-05	0.017248
HSPB1	-0.38434	9.410244	22.73045	1.86E-06	0.002714
CYB5R1	-0.38118	5.770637	15.1487	9.94E-05	0.022945
SLC2A6	-0.3756	4.189715	15.40244	8.69E-05	0.021651
MSRB1	-0.3701	5.511516	14.55164	0.00013637	0.027729
ENDOD1	-0.36543	6.610153	14.06412	0.000176682	0.032973
SIX2	-0.36102	5.707384	13.44129	0.000246147	0.038563
RAVER2	-0.35903	4.2544	19.80343	8.58E-06	0.005791
TUBB2A	-0.34554	5.187744	14.4532	0.000143686	0.02877
MIEN1	-0.34286	1.951609	13.04021	0.000304874	0.04321
RGS19	-0.33713	3.360489	12.52686	0.000401143	0.049474
PSEN2	-0.33481	4.018959	19.30059	1.12E-05	0.006177
GSN	-0.32799	9.22319	21.84951	2.95E-06	0.003444
MAP2K3	-0.32026	6.621549	25.12837	5.36E-07	0.000963
MGAT5	-0.30153	6.814577	15.61065	7.78E-05	0.020257
SNTA1	-0.29562	5.384169	12.61557	0.000382546	0.048707
PTPN3	-0.29194	3.537507	18.04734	2.15E-05	0.00947
SORT1	-0.29142	7.62097	16.69438	4.39E-05	0.014021
SRD5A1	-0.28284	4.729072	25.68423	4.02E-07	0.000853
TPST2	-0.28145	6.976341	18.20642	1.98E-05	0.008993
CALM1	-0.27529	8.260706	17.00462	3.73E-05	0.012807
ROGDI	-0.27022	4.824984	15.59218	7.86E-05	0.020327
DAB2IP	-0.26752	5.951331	17.01764	3.70E-05	0.012807
DIRAS1	-0.2544	5.512156	12.89333	0.000329755	0.045378
FAM219A	-0.25096	5.24701	21.62318	3.32E-06	0.003535
EHD1	-0.24981	7.699704	23.91399	1.01E-06	0.001584
BCAP31	-0.24721	7.121209	13.18563	0.000282103	0.041624
CTNNB1	-0.24353	8.746768	16.89087	3.96E-05	0.013263
RHOC	-0.23978	8.846199	13.7611	0.000207591	0.035238
HDAC5	-0.23914	5.900239	15.55691	8.01E-05	0.020579
INPP5A	-0.23369	5.185924	12.83613	0.00033999	0.046385
CUEDC1	-0.23047	6.109555	17.66143	2.64E-05	0.010735
LASP1	-0.22691	9.744295	18.35837	1.83E-05	0.008698
FEZ2	-0.22165	6.185835	13.57329	0.000229427	0.037658
IGHMBP2	-0.22138	4.300589	14.06617	0.00017649	0.032973
EMP3	-0.22047	7.715333	12.61791	0.000382068	0.048707

Continuation of the Table 4

Gene	logFC	logCPM	LR	p-value	FDR
PREB	-0.2187	5.839774	12.72631	0.000360548	0.048132
DDRGK1	-0.21732	5.515303	15.17375	9.81E-05	0.022901
HDAC11	-0.20866	4.352068	17.601	2.72E-05	0.010811
PITPNM1	-0.20846	5.371332	13.86789	0.000196121	0.0347
LDLRAP1	-0.20678	5.838397	13.05207	0.000302949	0.04321
ARHGEF10L	-0.20518	5.919073	12.77922	0.000350491	0.04727
NPTN	-0.20116	8.061508	14.95693	0.000109993	0.0243
SNX11	-0.20075	4.663461	17.13849	3.48E-05	0.01235
NAPA	-0.19531	4.064688	14.61631	0.000131769	0.027338
TMEM109	-0.19072	6.596263	14.83157	0.000117551	0.024893
SPRYD3	-0.18655	6.312584	12.77161	0.000351921	0.04727
MAPRE3	-0.17976	4.672064	12.48096	0.000411121	0.04986
KIF1C	-0.17932	8.266324	19.72121	8.96E-06	0.005907
PPP2CB	-0.17822	6.651028	16.61981	4.57E-05	0.014249
RHBDD2	-0.17806	5.673687	19.5745	9.68E-06	0.006084
SELENOS	-0.17695	6.242757	13.12572	0.00029127	0.042065
SLC27A4	-0.17567	5.214289	12.51806	0.000403037	0.049474
ARMCX3	-0.17348	6.995281	13.15464	0.000286808	0.041865
RMDN3	-0.16785	5.427733	13.50392	0.000238065	0.038058
LRRFIP2	-0.15981	6.355986	13.13037	0.000290548	0.042065
PPP2R1A	-0.15488	7.886332	12.99828	0.000311777	0.043789
SEC14L1	-0.15293	6.814728	15.27059	9.32E-05	0.022663
EHBP1L1	-0.14069	7.671404	14.1189	0.000171611	0.032848
BLCAP	-0.13762	6.3339	13.40166	0.000251401	0.039069
LZTS2	-0.13014	6.888952	12.78966	0.000348541	0.04727
GART	0.144891	5.426869	16.73461	4.30E-05	0.013937
NUDT21	0.146174	5.944158	12.67975	0.000369637	0.048132
PTGR3	0.151359	4.48144	12.68544	0.000368514	0.048132
HEATR6	0.168375	4.60623	16.04382	6.19E-05	0.017446
PSIP1	0.174873	5.351493	12.7672	0.00035275	0.04727
CMTR2	0.176201	4.585269	17.05302	3.64E-05	0.012756
RAD21	0.190763	5.803668	12.67307	0.00037096	0.048132
FUT8	0.197327	5.011198	12.5474	0.000396759	0.049474
CARD8	0.223999	3.931231	16.5491	4.74E-05	0.014568
S100PBP	0.246188	4.671997	20.87633	4.90E-06	0.004005
USP28	0.249203	4.178656	20.00123	7.74E-06	0.005454
BDH2	0.253192	3.366615	14.47918	0.000141717	0.028533
CASP4	0.256899	4.924556	20.10625	7.33E-06	0.005253
ZCCHC8	0.260018	4.188864	20.62361	5.59E-06	0.004311
B4GALT5	0.262408	5.952676	14.25092	0.000159983	0.031285
IRAK1BP1	0.275405	2.588981	13.84753	0.000198258	0.034817
IFI16	0.278147	6.395011	14.08274	0.000174942	0.032973
AMMECR1	0.278167	4.031016	13.71351	0.000212917	0.035959
SH2D4A	0.295128	5.667351	13.02964	0.000306599	0.04321

Continuation of the Table 4

Gene	logFC	logCPM	LR	p-value	FDR
DPH5-DT	0.301347	2.46994	16.22833	5.61E-05	0.016806
TMEM116	0.310949	2.121463	13.07266	0.000299638	0.04297
DPYD	0.325722	5.376649	13.1719	0.000284178	0.041779
SRPX	0.330869	5.435651	18.19592	1.99E-05	0.008993
ARHGEF3	0.366546	2.935045	16.02308	6.26E-05	0.017517
SERAC1	0.374418	5.547421	16.32552	5.33E-05	0.016149
CDK14	0.379537	5.705607	16.07847	6.08E-05	0.017248
GLT8D2	0.386548	4.708298	16.93926	3.86E-05	0.013037
ESR1	0.387471	1.004918	13.63949	0.000221478	0.036797
FGF2	0.388723	4.715732	17.35999	3.09E-05	0.011813
PLSCR1	0.393244	3.954516	19.12633	1.22E-05	0.006494
RUNX1T1	0.395472	3.164303	13.35076	0.000258318	0.039691
IGFBP3	0.398171	12.15029	16.00963	6.30E-05	0.017522
FMNL2	0.401245	4.579389	13.79527	0.000203849	0.035154
ZEB1-AS1	0.405514	1.250406	16.35924	5.24E-05	0.015982
RHOBTB3	0.421879	4.703756	19.29777	1.12E-05	0.006177
PTPRE	0.456301	2.718066	15.96502	6.45E-05	0.017804
OR2A1-AS1	0.460911	0.345043	14.55567	0.000136078	0.027729
MISFA	0.467977	-0.147	12.54327	0.000397636	0.049474
SIM2	0.487467	2.960039	16.63429	4.53E-05	0.014249
CELF6	0.557284	-0.13149	16.17211	5.78E-05	0.016806
ABCA12	0.579788	0.062118	14.17864	0.000166247	0.032202
SEMA5A	0.582161	6.489798	17.20552	3.35E-05	0.01235
IRS2	0.591112	4.466242	14.10983	0.00017244	0.032848
LINC01277	0.786045	-0.53122	14.16108	0.000167806	0.032351
ZFPM2	0.801454	0.340995	12.91085	0.000326684	0.045108
TWIST2	0.831999	4.611952	12.65027	0.000375512	0.048415
KCNK15	0.843858	2.00907	16.57159	4.68E-05	0.014505
LYPLAL1-AS1	0.870673	-0.54629	20.83813	5.00E-06	0.004005
CTSK	0.892649	4.827643	20.56693	5.76E-06	0.004358
RARRES1	0.89793	1.201195	33.30716	7.87E-09	4.59E-05
CELSR1	0.899855	3.295554	12.7837	0.000349652	0.04727
EPHA3	0.942838	2.566101	16.95059	3.84E-05	0.013037
LINC00906	0.952773	-1.22901	19.67965	9.16E-06	0.005941
DENND2A	0.959001	0.240724	13.41387	0.00024977	0.038963
EIF4A2P3	1.000457	-1.55854	14.77132	0.000121367	0.025479
ABCA6	1.018584	2.061196	13.22672	0.000275986	0.041179
USP6	1.140794	-0.65042	13.33082	0.000261079	0.039816
C3	1.160315	4.277584	13.64326	0.000221033	0.036797
FOLR3	1.242528	-1.2425	14.01678	0.000181187	0.033347
LHX9	1.30102	1.764174	32.56135	1.15E-08	5.24E-05
ST3GAL6-AS1	1.400417	-2.06166	12.94407	0.000320936	0.044663
LINC02385	1.512722	-1.89567	18.89287	1.38E-05	0.007153

Gene	logFC	logCPM	LR	p-value	FDR
SLC15A5	1.512989	-1.98155	17.51228	2.85E-05	0.011007
CASP16P	1.513554	-2.07019	13.84536	0.000198486	0.034817
CNTNAP3B	1.785434	2.465226	16.2065	5.68E-05	0.016806
ZNF232	3.397878	-2.27352	14.85184	0.000116294	0.024756

Table 5 Performance of predictive models based on LASSO regression and RFR for chronological age estimation

	R	FR	LASSO		
Indicators	Pearson correlation coefficient	Spearman correlation coefficient	Pearson correlation coefficient	Spearman correlation coefficient	
Number of genes (r> 0.5)	26	135	26	135	
MAE	10.516	10.060	9.858	12.731	
R ²	0.684	0.742	0.755	0.655	

Table 6 Performance of predictive models based on LASSO regression and RFR for the assessment of in vitro culture duration (passage number)

	R	FR	LASSO		
Indicators	Pearson correlation coefficient	Spearman correlation coefficient	Pearson correlation coefficient	Spearman correlation coefficient	
Number of genes (r> 0.5)	26	186	26	186	
MAE	0.490	0.440	0.508	0.682	
\mathbb{R}^2	0.261	0.323	0.583	0.267	

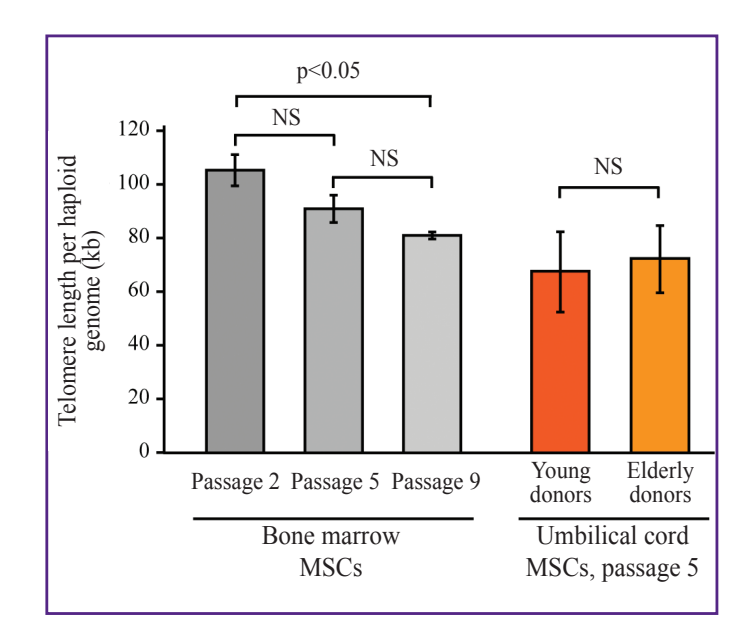


Figure 2. Comparison of the absolute telomere length normalized to the haploid genome in cultured MSCs

Measurements were performed using quantitative PCR. The telomere length was compared between the umbilical MSCs at different passages and between the donor bone marrow MSCs isolated from the young (20-25 years, n=3) and elderly (>60 years, n=3) donors. NS — p≥0.05, Student's t-test

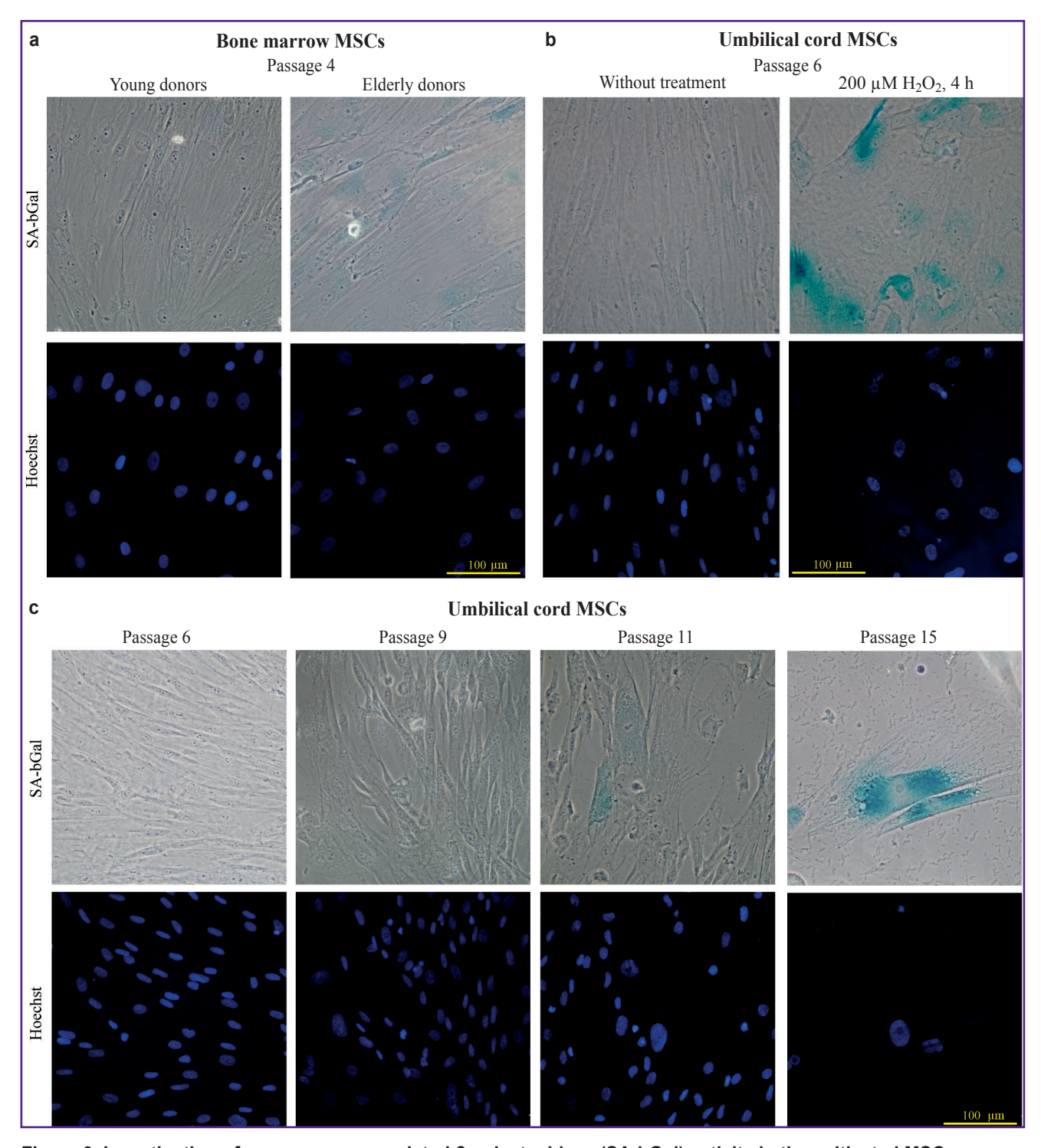


Figure 3. Investigation of senescence associated β-galactosidase (SA-bGal) activity in the cultivated MSCs Cells were fixed and stained to determine SA-bGal, nuclear DNA was stained with the Hoechst dye; (a) comparison of bone marrow MSCs from the young (18-25 years) and elderly (>65 years) donor at cultivation passage 4; (b) comparison of umbilical cord MSCs at passage 6 under standard cultivation conditions and after a 4-hour treatment of 200 µM solution of hydrogen peroxide; (c) comparison of umbilical cord MSCs at cultivation passages 6, 9, 11, and 15 under standard cultivation conditions

Moreover, we did not find significant differences comparing cell preparations from the donors of various ages (see Figure 4 (c), (d)). However, at the level of nuclear morphology, the reduction of H3K9me3 signal intensity was noted, which agrees with heterochromatin erosion observed in aging, and enlargement of nuclei

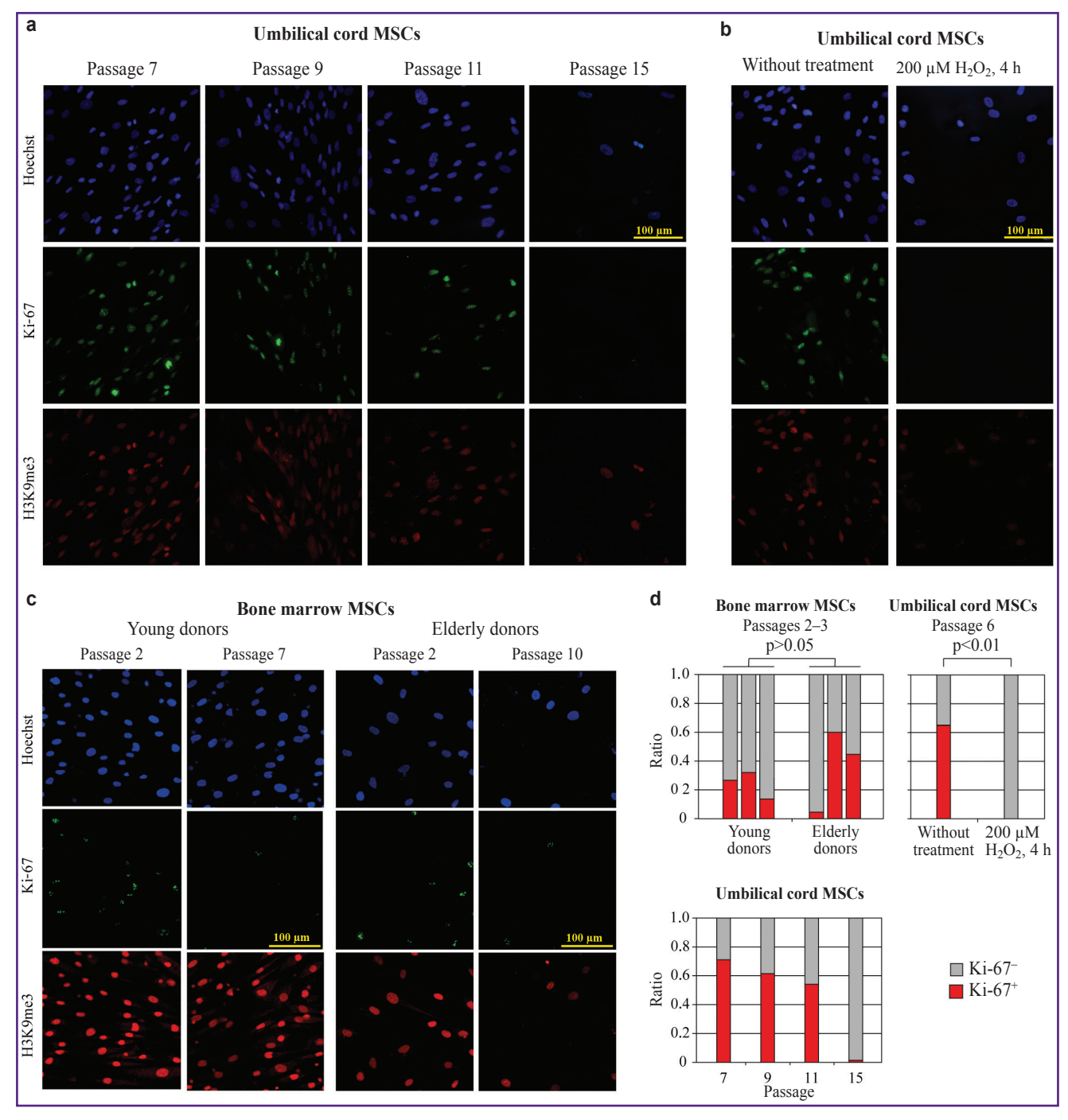


Figure 4. Investigations of the nuclear marker Ki-67 in the MSC cultures

Formaldehyde-fixed MSC samples were stained with antibodies against the cell proliferation marker Ki-67 (a)–(c), the rate of Ki-67-positive nuclei on the samples was then determined (d). For visualization of nuclei, chromatin was stained with antibodies against histone modification H3K9me3, nuclear DNA was stained with Hoechst; (a) comparison of umbilical cord MSCs at passages 7, 9, 11, and 15; (b) comparison of umbilical cord MSCs at passage 6 under standard conditions and after 4-hour treatment of 200 µM solution of hydrogen peroxide; (c) comparison of staining the donor bone marrow MSCs at early and late cultivation passages; (d) the rate of Ki-67-positive cells on the stained MSC samples

was observed at later passages and with increase of the donor age. Similar effects were also noted during continuous cultivation and stress-induced senescence of the umbilical cord MSCs (see Figure 4 (a)-(c)).

It is interesting to note that an increasing amount of

evidence is accumulating in favor of using changes in nuclear morphology as an independent marker of cellular senescence. From the technical point of view, this analysis looks robust, since it actually requires microscopic analysis coupled with fluorescent nuclear

staining. Moreover, available approaches in the machine learning image recognition accelerate processing and collection of the required statistical data. For this reason, to systematically analyze changes in nuclear morphology during aging, we trained a segmentation neural network model that describes nuclear morphology parameters such as area, roundness, and ellipse parameters (see "Materials and Methods"). The model demonstrated high segmentation quality on the test set (Figure 5 (a)), As the primary metric for evaluating model performance,

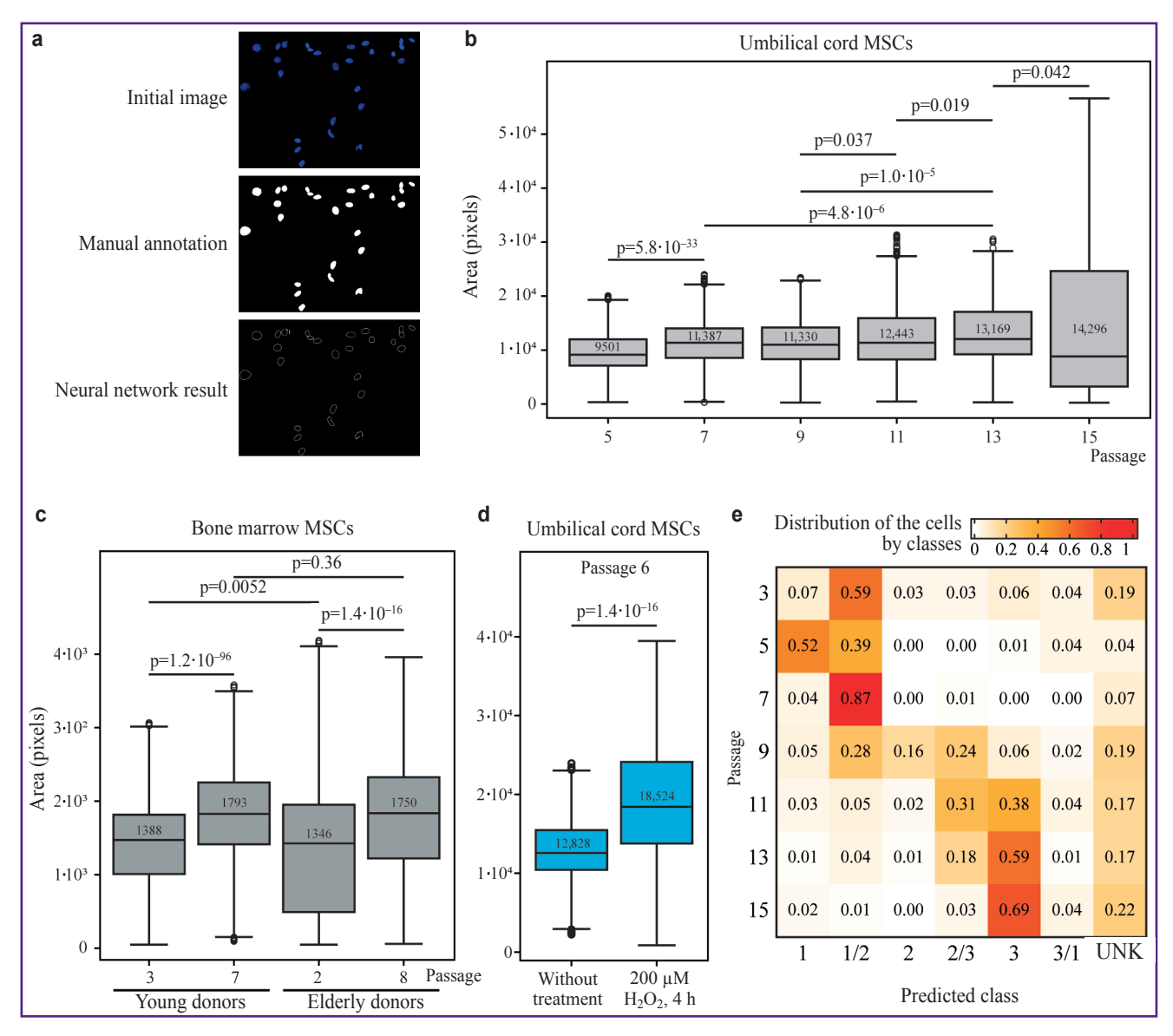


Figure 5. Investigation of the MSC samples using neural network algorithm for image segmentation and classification

The image segmentation algorithm was trained based on the stained MSC samples, (a) upper image. For training the neural network, nuclear boundaries on the samples were manually annotated, (a) middle image. The trained algorithm successfully identified the nucleus boundaries, (a) lower image. The segmentation algorithm was subsequently used to estimate the sizes of MSC nuclei during passaging or under stress conditions (b, c, d), as well as for subsequent classification of cells into age classes (e). Figure (b) comparison of the nuclear areas in umbilical cord MSCs samples at passages 5, 7, 9, 11, 13, and 15; (c) comparison of nuclear areas in donor bone marrow MSCs samples at early and late cultivation passages; (d) comparison of the nuclear areas in umbilical cord MSC samples under standard cultivation conditions and after the 4-hour treatment of 200 µM solution of hydrogen peroxide; the numbers show mean area values; statistically significant differences were calculated using the Mann-Whitney test. Figure (e) a heat map of cell distribution across predicted classes in MSC samples from different passages. The neural network algorithm assigned cells to three classes: class 1 corresponded to early passages, class 2 to intermediate passages, class 3 to late passages. Cells that had an equal probability of belonging to two classes were assigned the value 1/2, 2/3, or 3/1. Cells for which a class could not be unambiguously determined were assigned the value "Unknown" (UNK)

ADVANCED RESEARCHES

the Intersection over Union (IoU) measure was used. The IoU obtained for the model, equal to 0.88, indicates effective segmentation of cell nuclei and their boundaries even in the presence of noise and variations in the original images. For each nucleus, a set of parameters was calculated:

- 1) the center coordinates (X, Y) allow the nucleus to be matched with other cellular structures and used for spatial analysis; they are defined as the centroid derived from contour moments:
- area a marker of the overall size of the nucleus. an increase in area can be associated with cells transitioning to later passages;
- 3) roundness characterizes shape compactness. an increase in the value indicates that the nucleus is acquiring a more circular shape, which may be associated with later stages of cellular senescence;
- 4) the ellipse semi-axes and orientation angle allow assessment of the degree of elongation and the nucleus
- 5) the Hausdorff distance serves as a criterion of approximation quality, low values (<10) indicate that the nucleus shape conforms to an ellipse.

Using the developed model, data on the size and shape of MSCs nuclei (Figure 5 (b)-(d)) from the donors of various ages (n=9308), subjected to varying the duration of in vitro cultivation (n=5157), and before and after the induction of stress-mediated cell senescence (n=564) were collected. Cells from donors in the older age group showed a broader range of nuclear sizes at the early stages of culture, whereas with increasing passage the nuclear sizes of cells from donors of different ages converged (see Figure 5 (c)). During prolonged culture the nuclear size also increased significantly, and this increase occurred gradually (see Figure 5 (b)). Stressinduced senescence was associated with the most dramatic increase in nuclear size (see Figure 5 (d)).

At the next step, we evaluated the possibility of predicting the duration of cell cultivation, expressed as the ordinal number of the cultural passage, from nuclear morphology. The developed model classified the cells into three classes: early cultural passages (passages 3-5), intermediate (passages 7-9), and late (passages 11–15) according to the structure of the training dataset. As a result of the model's operation, the analyzed cells were assigned a membership coefficient for one of the listed classes. The algorithm for calculating classmembership coefficients comprised several stages. At the first stage, a cell region was generated by merging the boundary mask with the class masks; then, based on the segmentation results, the cell contour was extracted and filled. The next stage involved counting overlaps with the class masks to determine the number of pixels that simultaneously lay within the cell region and the mask of the corresponding class. Subsequently, normalization by cell area was performed, whereby for each class the ratio of overlapping pixels to the total cell area was converted into a proportion ranging from 0 to

100%. These proportions were then adjusted so that their sum equaled 100%, and the corrected proportions were taken as the membership-coefficient values for each class. Membership to the primary classes (1, 2, 3) was defined by the highest coefficient value; a mixed class (1/2, 2/3, 3/1) was assigned when the difference between the coefficients of two classes did not exceed 10%; an undefined class was assigned to a cell when the coefficients for all classes were close to each other (all values below 40%). Evaluation of the algorithm on the test set demonstrated adequate prediction of the actual culture passages of the studied cells (Figure 5 (e)). Starting from passage 9, the representation of cells in different classes increased, which may be related to rising morphological heterogeneity of cells associated with aging. With increasing passage number in the test sample, the proportion of cells classified as late-passage cells steadily grew, most likely reflecting the dynamics of accumulation of senescent cells.

Discussion

The key hallmark of cellular senescence is an irreversible arrest of the cell cycle mediated by the activation of cyclin-dependent kinase p16INK4a and p21CIP1a [3]. In the studied models of MSC cellular senescence, the genes encoding the proteins p16INK4a, p21CIP1a also displayed the expected dynamics. Moreover, substantial changes occurred in cell morphology and nuclear architecture. A significant role in the alteration of nuclear and chromatin structure is played by the senescence-associated decrease in the expression level of LMNB1 gene [15, 34]. The reduction of the LMNB1 gene expression level was observed in all examined models of cellular aging and it was most pronounced in the replicative senescence of MSCs. Specific changes in chromatin structure also include the formation of the so-called senescenceassociated heterochromatin domains (SAHF and SAHD) together with decondensation of peri/centromeric heterochromatin regions (SADS) and global erosion of heterochromatin [16, 35-37]. These changes are involved in the regulation of both genes comprising the so-called senescence-associated proinflammatory phenotype [14, 35].

One of the factors determining the chromatin structure is a nuclear architectural protein, HMGB2, whose expression declines during cellular senescence and which, in particular, is considered as an early marker of cellular senescence [14, 38]. A decrease in the expression of the HMGB2 gene was also detected with the increase of chronological age of MSC donors, in stress-induced and replicative senescence of MSCs. In the oncogene-induced senescence model HMGB2 has been shown to prevent propagation of heterochromatin in the genome regions containing genes forming the so-called senescence-associated proinflammatory phenotype, thereby helping

maintain their expression [14]. Although such an effect has not been confirmed in the replicative senescence, however, the development of a more permissive chromatin state during aging — caused by disruptions of the machinery that maintains facultative and constitutive heterochromatin, remodeling of the nuclear spatial topology, and activation of intracellular pro-inflammatory signaling pathways in response to DNA damage (cGAS-STING) — are key factors that determine the formation of the SASP [15, 37, 39].

The concept of senescence-associated secretory phenotype unites the complex of proinflammatory cytokines, growth factors, and metalloproteinases [40]. The main factors that constitute the SASP are TNFα. MCP-1, MCP-2, SERPINE1/PAI-1, GM-CSF, GROα, β, γ, IGFBP-7, interleukins IL-1α, IL-6, IL-7, IL-8, chemokine MIP1α, and matrix metaloproteinases MMP-1, MMP-10, and MMP-3 [41]. However, it is important to note that the composition of SASP changes significantly depending on the cause of cellular senescence and the cell type [18]. Interestingly, when comparing MSCs from donors of different ages, no significant dynamics in the expression of genes encoding individual interleukins was detected. At the same time, during culture and under stressinduced senescence, pro-inflammatory SASP factors such as IL-6, CXCL8, IL-1β became activated. This observation partially contradicts the previous reports of increased activity of these SASP factors in MSCs from older donors [42]. It should be emphasized, however, that in the cited study, a convincing difference in expression was demonstrated only for IL-6. Moreover, our analysis of published transcriptomes of BM-MSC samples (n=37) did not find reliable correlation between the expression of the investigated genes encoding individual SASP components and the age. All this together may reflect the heterogeneity and substantial contribution of donor-specific effects that complicate the analysis of age-related changes of gene expression. This is also supported by the performance of the regression model for predicting chronological age, which exhibited a relatively high value of the mean absolute error (R²=0.755; MAE=9.858 years).

It should be noted that previously described predictive models for estimating age from transcriptomic data have demonstrated comparable effectiveness [20, 43, 44]. More accurate similar algorithms generally achieve maximum performance on the narrow age cohorts. Moreover, in the process of model development, the authors excluded multiple available samples from the analysis, since their inclusion significantly worsened the model quality [45]. Thus, the evaluation of gene expression dynamics may be used to the greater extent to analyze cellular senescence in vitro. In this case, typically only limited number of cell lines are investigated under relatively standard cultivation conditions, which is likely to reduce the variability of gene expression profiles inherent to the primary donor cell cultures and samples. Similarly, according to the data obtained by

us, the assessment of MSC telomere length, at least on the small sample sets, is also rather applicable for the evaluation of replicative senescence in vitro.

Cytological analysis techniques are widely used to study cellular senescence. Cellular senescence is accompanied by characteristic morphological changes such as flattening, enlargement of the cell and nuclear size, as well as the appearance of specific protein markers, like activation of senescence-associated β-galactosidase [3, 46]. In the present work, the activity of senescence-associated β-galactosidase demonstrated its applicability for the qualitative assessment of both replicative and stress-induced senescence. However, the use of this marker for the evaluation of the functional state of the cells requires standardization of several conditions. First, it is necessary to control the efficiency of the reagent lot used in the work, since the pH shift of these reagents may essentially distort the results. Taking into account the necessity to analyze the freshly prepared cell slides, it is not always feasible in serial experiments conducted in research laboratories. Besides, cell preparations must demonstrate similar cell density, since the elevated confluence can lead to distorted results [47]. Interpretation of the obtained results at the early stages of the cellular senescence may be difficult due to the absence of a fixed threshold value of the β-galactosidase activity, making it difficult to classify cells as positive or negative for this marker. Altogether, this limits the application of this marker for studying cell preparations obtained from donors of various ages.

As an alternative, approaches to assessing cellular aging based on the analysis of several protein markers associated with proliferation, apoptosis, and DNA damage may be considered [17]. At the same time, the applicability of these approaches is again limited by the selection of optimal markers. For example, expression of the protein Ki-67 widely used as a proliferation marker depends on the stage of the cell cycle, while the variant of yH2Ax histone, the marker of the DNA damage, is detected at the late stages of cellular senescence [17, 48].

With the development of the machine learning methods, there was proposed a concept, according to which the processive analysis of cell morphology may serve as an integral metric of cell aging [21, 49, 50]. To estimate the applicability to this approach, we have developed a segmentation neural network model for the automated assessment of the nuclear morphology parameters. The analysis of BM-MSCs from the donors of various ages at the early passages has shown that the range of nucleus sizes was wider in the cell sample of the donors from the older age group. The nucleus size gradually increased during MSC cultivation and the size of the BM-MSC nuclei from the donors of various ages did not demonstrate significant differences between the age groups. The most prominent change of the nuclear morphology was observed in stressinduced cell senescence. The developed model also allows for effective classification of the individual cell passage as a surrogate metric of the cell aging stage for umbilical cord MSC samples. In this connection, it may be supposed to be also employed for the estimation of the functional state of the donor BM-MSC samples if there is a sufficient amount of datasets for the training sample. Besides, the application of similar models to assess the effects directed to the reduction of cell senescence manifestations, such as rejuvenation by partial reprogramming is of great interest [51, 52].

Conclusion

In the presented work, some aspects of phenotypic manifestations of various types of MSC senescence have been studied. At the level of individual gene expression, it has been shown that the change in the expression levels of CDKN1A, LMNB1, HMGB2, and SERPINE1/PAI1 is observed in all investigated models of cellular senescence. At the same time, the analysis of transcriptomic data has demonstrated significant donor-dependent heterogeneity of gene expression profiles, which hampers creation of effective predictive models for the evaluation of chronological age and the duration of the in vitro cultivation. At the same time, an alternative predictive metric of cellular aging — at least in the case of replicative aging — can be changes in nuclear morphology, whose dynamic analysis using neural-network models allows us to estimate the duration of in vitro cultivation. Combining such approaches with other promising metrics, such as epigenetic clock algorithms, gives hope for developing functional algorithms to evaluate the phenomenon of cellular senescence.

Research funding. The work was financially supported by the Russian Science Foundation. Research Project No.22-74-10123.

Conflicts of interest. The authors declare no conflicts of interest.

References

- 1. Margiana R., Markov A., Zekiy A.O., Hamza M.U., Al-Dabbagh K.A., Al-Zubaidi S.H., Hameed N.M., Ahmad I., Sivaraman R., Kzar H.H., Al-Gazally M.E., Mustafa Y.F., Siahmansouri H. Clinical application of mesenchymal stem cell in regenerative medicine: a narrative review. Stem Cell Res Ther 2022; 13(1): 366, https://doi.org/10.1186/s13287-022-03054-0.
- 2. Galderisi U., Peluso G., Di Bernardo G. Clinical trials based on mesenchymal stromal cells are exponentially increasing: where are we in recent years? Stem Cell Rev Rep 2022; 18(1): 23-36, https://doi.org/10.1007/s12015-021-10231-w.
- 3. Campisi J., d'Adda di Fagagna F. Cellular senescence: when bad things happen to good cells. Nat Rev Mol Cell Biol 2007; 8(9): 729-740, https://doi.org/10.1038/ nrm2233.

- 4. Zha K., Li X., Yang Z., Tian G., Sun Z., Sui X., Dai Y., Liu S., Guo Q. Heterogeneity of mesenchymal stem cells in cartilage regeneration: from characterization to application. NPJ Regen Med 2021; 6(1): 14, https://doi.org/10.1038/ s41536-021-00122-6.
- 5. Alm J.J., Qian H., Le Blanc K. Chapter 13 Clinical grade production of mesenchymal stromal cells. In: Tissue engineering. Elsevier; 2014; p. 427-469, https://doi. org/10.1016/B978-0-12-420145-3.00013-4.
- 6. Xiang S., Gao W., Peng H., Liu A., Ao Q., Yang M., Yu Y., Liu Y., Rong R. Standards of clinical-grade mesenchymal stromal cell preparation and quality control (2020 China version). J Neurorestoratol 2020; 8(4): 197-216, https://doi.org/10.26599/JNR.2020.9040021.
- 7. López-Otín C., Blasco M.A., Partridge L., Serrano M., Kroemer G. Hallmarks of aging: an expanding universe. Cell 2023; 186(2): 243–278, https://doi.org/10.1016/j. cell.2022.11.001.
- 8. Kuilman T., Michaloglou C., Mooi W.J., Peeper D.S. The essence of senescence. Genes Dev 2010; 24(22): 2463-2479, https://doi.org/10.1101/gad.1971610.
- 9. Pazolli E., Alspach E., Milczarek A., Prior J., Piwnica-Worms D., Stewart S.A. Chromatin remodeling underlies the senescence-associated secretory phenotype of tumor stromal fibroblasts that supports cancer progression. Cancer Res 2012; 72(9): 2251-2261, https://doi.org/10.1158/0008-5472.CAN-11-3386.
- 10. Mikuła-Pietrasik J., Niklas A., Uruski P., Tykarski A., Książek K. Mechanisms and significance of therapy-induced and spontaneous senescence of cancer cells. Cell Mol Life Sci 2020; 77(2): 213–229, https://doi.org/10.1007/s00018-019-03261-8.
- **11.** Kumari R., Jat P. Mechanisms of cellular senescence: cell cycle arrest and senescence associated secretory phenotype. Front Cell Dev Biol 2021; 9: 645593, https://doi. org/10.3389/fcell.2021.645593.
- 12. González-Gualda E., Baker A.G., Fruk L., Muñoz-Espín D. A guide to assessing cellular senescence in vitro and in vivo. FEBS J 2021; 288(1): 56-80, https://doi. org/10.1111/febs.15570.
- **13.** Carnero A. Markers of cellular senescence. *Methods* Mol Biol 2013; 965: 63-81, https://doi.org/10.1007/978-1-62703-239-1 4.
- 14. Aird K.M., Iwasaki O., Kossenkov A.V., Tanizawa H., Fatkhutdinov N., Bitler B.G., Le L., Alicea G., Yang T.L., Johnson F.B., Noma K.I., Zhang R. HMGB2 orchestrates the chromatin landscape of senescence-associated secretory phenotype gene loci. J Cell Biol 2016; 215(3): 325-334, https://doi.org/10.1083/jcb.201608026.
- 15. Shah P.P., Donahue G., Otte G.L., Capell B.C., Nelson D.M., Cao K., Aggarwala V., Cruickshanks H.A., Rai T.S., McBryan T., Gregory B.D., Adams P.D., Berger S.L. Lamin B1 depletion in senescent cells triggers largescale changes in gene expression and the chromatin landscape. Genes Dev 2013; 27(16): 1787-1799, https://doi. org/10.1101/gad.223834.113.
- 16. Criscione S.W., Teo Y.V., Neretti N. The chromatin landscape of cellular senescence. Trends Genet 2016; 32(11): 751-761, https://doi.org/10.1016/j.tig.2016.09.005.
- 17. Galvis D., Walsh D., Harries L.W., Latorre E., Rankin J. A dynamical systems model for the measurement

- of cellular senescence. J R Soc Interface 2019; 16(159): 20190311, https://doi.org/10.1098/rsif.2019.0311.
- 18. Coppé J.P., Desprez P.Y., Krtolica A., Campisi J. The senescence-associated secretory phenotype: the dark side of tumor suppression. Annu Rev Pathol 2010; 5: 99-118, https://doi.org/10.1146/annurev-pathol-121808-102144.
- 19. Simpson D.J., Chandra T. Epigenetic age prediction. Aging Cell 2021; 20(9): e13452, https://doi.org/10.1111/ acel.13452.
- 20. Mamoshina P., Volosnikova M., Ozerov I.V., Putin E., Skibina E., Cortese F., Zhavoronkov A. Machine learning on human muscle transcriptomic data for biomarker discovery and tissue-specific drug target identification. Front Genet 2018; 9: 242, https://doi.org/10.3389/fgene.2018.00242.
- 21. Heckenbach I., Mkrtchyan G.V., Ezra M.B., Bakula D., Madsen J.S., Nielsen M.H., Oró D., Osborne B., Covarrubias A.J., Idda M.L., Gorospe M., Mortensen L., Verdin E., Westendorp R., Scheibye-Knudsen M. Nuclear morphology is a deep learning biomarker of cellular senescence. Nat Aging 2022; 2(8): 742-755, https://doi. org/10.1038/s43587-022-00263-3.
- 22. Debacq-Chainiaux F., Erusalimsky J.D., Campisi J., Toussaint O. Protocols to detect senescence-associated beta-galactosidase (SA-betagal) activity, a biomarker of senescent cells in culture and in vivo. Nat Protoc 2009; 4(12): 1798–1806, https://doi.org/10.1038/nprot.2009.191.
- 23. Andrzejewska A., Catar R., Schoon J., Qazi T.H., Sass F.A., Jacobi D., Blankenstein A., Reinke S., Krüger D., Streitz M., Schlickeiser S., Richter S., Souidi N., Beez C., Kamhieh-Milz J., Krüger U., Zemojtel T., Jürchott K., Strunk D., Reinke P., Duda G., Moll G., Geissler S. Multiparameter analysis of biobanked human bone marrow stromal cells shows little influence for donor age and mild comorbidities on phenotypic and functional properties. Front Immunol 2019; 10: 2474, https://doi.org/10.3389/ fimmu.2019.02474.
- 24. Ayhan S., Nemutlu E., Uçkan Çetinkaya D., Kır S., Özgül R.K. Characterization of human bone marrow niches with metabolome and transcriptome profiling. J Cell Sci 2021; 134(6): jcs250720, https://doi.org/10.1242/ ics.250720.
- 25. Li H., Handsaker B., Wysoker A., Fennell T., Ruan J., Homer N., Marth G., Abecasis G., Durbin R; 1000 Genome Project Data Processing Subgroup. The sequence alignment/ Map format and SAMtools. Bioinformatics 2009; 25(16): 2078-2079, https://doi.org/10.1093/bioinformatics/btp352.
- 26. Dobin A., Davis C.A., Schlesinger F., Drenkow J., Zaleski C., Jha S., Batut P., Chaisson M., Gingeras T.R. STAR: ultrafast universal RNA-seq aligner. Bioinformatics 2013; 29(1): 15-21, https://doi.org/10.1093/bioinformatics/ bts635.
- 27. Liao Y., Smyth G.K., Shi W. featureCounts: an efficient general purpose program for assigning sequence reads to genomic features. Bioinformatics 2014; 30(7): 923-930, https://doi.org/10.1093/bioinformatics/btt656.
- 28. Zhang Y., Parmigiani G., Johnson W.E. ComBatseq: batch effect adjustment for RNA-seq count data. NAR Genomics and Bioinformatics 2020; 2(3), https://doi. org/10.1093/nargab/lqaa078.
- 29. Robinson M.D., McCarthy D.J., Smyth G.K. edgeR: a bioconductor package for differential expression analysis

- of digital gene expression data. Bioinformatics 2010; 26(1): 139–140. https://doi.org/10.1093/bioinformatics/btp616.
- 30. Pedregosa F., Varoquaux G., Gramfort A., Michel V., Thirion B., Grisel O., Blondel M., Prettenhofer P., Weiss R., Dubourg V., Vanderplas J., Passos A., Cournapeau D., Brucher M., Perrot M., Duchesnay E. Scikit-learn: machine learning in Python. Journal of Machine Learning Research 2011; 12: 2825-2830.
- 31. Kirillov A., Mintun E., Ravi N., Mao H., Rolland C., Gustafson L., Xiao T., Whitehead S., Berg A.C., Lo W.-Y., Dollár P., Girshick R. Segment anything. In: 2023 IEEE/CVF International Conference on Computer Vision (ICCV), 2023. https://doi.org/10.1109/iccv51070.2023.00371.
- 32. Chen L.C., Zhu Y., Papandreou G., Schroff F., Adam H. Encoder-decoder with atrous separable convolution for semantic image segmentation. In: Ferrari V., Hebert M., Sminchisescu C., Weiss Y. (editors). Computer Vision — ECCV 2018. ECCV 2018. Lecture Notes in Computer Science, vol. 11211. Springer, Cham; 2018, https://doi. org/10.1007/978-3-030-01234-2 49.
- 33. Tan M., Le Q. EfficientNet: rethinking model scaling for convolutional neural networks. In: Le Proceedings of the 36th International Conference on Machine Learning, PMLR 2019: 97: 6105-6114.
- 34. Freund A., Laberge R.M., Demaria M., Campisi J. Lamin B1 loss is a senescence-associated biomarker. Mol Biol Cell 2012; 23(11): 2066-2075, https://doi.org/10.1091/ mbc.E11-10-0884.
- 35. Narita M., Nunez S., Heard E., Narita M., Lin A.W., Hearn S.A., Spector D.L., Hannon G.J., Lowe S.W. Rbmediated heterochromatin formation and silencing of E2F target genes during cellular senescence. Cell 2003; 113(6): 703-716, https://doi.org/10.1016/s0092-8674(03)00401-x.
- 36. Sati S., Bonev B., Szabo Q., Jost D., Bensadoun P., Serra F., Loubiere V., Papadopoulos G.L., Rivera-Mulia J.C., Fritsch L., Bouret P., Castillo D., Gelpi J.L., Orozco M., Vaillant C., Pellestor F., Bantignies F., Marti-Renom M.A., Gilbert D.M., Lemaitre J.M., Cavalli G. 4D genome rewiring during oncogene-induced and replicative senescence. Mol Cell 2020; 78(3): 522-538.e9, https://doi.org/10.1016/j. molcel.2020.03.007.
- 37. Dasgupta N., Arnold R., Equey A., Gandhi A., Adams P.D. The role of the dynamic epigenetic landscape in senescence: orchestrating SASP expression. NPJ Aging 2024; 10(1): 48, https://doi.org/10.1038/s41514-024-00172-2.
- 38. Zirkel A., Nikolic M., Sofiadis K., Mallm J.P., Brackley C.A., Gothe H., Drechsel O., Becker C., Altmüller J., Josipovic N., Georgomanolis T., Brant L., Franzen J., Koker M., Gusmao E.G., Costa I.G., Ullrich R.T., Wagner W., Roukos V., Nürnberg P., Marenduzzo D., Rippe K., Papantonis A. HMGB2 loss upon senescence entry disrupts genomic organization and induces CTCF clustering across cell types. Mol Cell 2018; 70(4): 730-744.e6, https://doi. org/10.1016/j.molcel.2018.03.030.
- 39. Miller K.N., Dasgupta N., Liu T., Adams P.D., Cytoplasmic chromatin fragments-from M.G. mechanisms to therapeutic potential. Elife 2021; 10: e63728, https://doi.org/10.7554/eLife.63728.
- 40. Coppé J.P., Patil C.K., Rodier F., Sun Y., Muñoz D.P., Goldstein J., Nelson P.S., Desprez P.Y., Campisi J.

ADVANCED RESEARCHES

- Senescence-associated secretory phenotypes reveal cellnonautonomous functions of oncogenic RAS and the p53 tumor suppressor. PLoS Biol 2008; 6(12): 2853-2868, https://doi.org/10.1371/journal.pbio.0060301.
- 41. Freund A., Orjalo A.V., Desprez P.Y., Campisi J. Inflammatory networks during cellular senescence: causes and consequences. Trends Mol Med 2010; 16(5): 238-246, https://doi.org/10.1016/j.molmed.2010.03.003.
- 42. Gnani D., Crippa S., Della Volpe L., Rossella V., Conti A., Lettera E., Rivis S., Ometti M., Fraschini G., Bernardo M.E., Di Micco R. An early-senescence state in aged mesenchymal stromal cells contributes to hematopoietic stem and progenitor cell clonogenic impairment through the activation of a pro-inflammatory program. Aging Cell 2019; 18(3): e12933, https://doi. org/10.1111/acel.12933.
- 43. Peters M.J., Joehanes R., Pilling L.C., Schurmann C., Conneely K.N., Powell J., Reinmaa E., Sutphin G.L., Zhernakova A., Schramm K., Wilson Y.A., Kobes S., Tukiainen T.; NABEC/UKBEC Consortium; Ramos Y.F., Göring H.H., Fornage M., Liu Y., Gharib S.A., Stranger B.E., De Jager P.L., Aviv A., Levy D., Murabito J.M., Munson P.J., Huan T., Hofman A., Uitterlinden A.G., Rivadeneira F., van Rooij J., Stolk L., Broer L., Verbiest M.M., Jhamai M., Arp P., Metspalu A., Tserel L., Milani L., Samani N.J., Peterson P., Kasela S., Codd V., Peters A., Ward-Caviness C.K., Herder C., Waldenberger M., Roden M., Singmann P., Zeilinger S., Illig T., Homuth G., Grabe H.J., Völzke H., Steil L., Kocher T., Murray A., Melzer D., Yaghootkar H., Bandinelli S., Moses E.K., Kent J.W., Curran J.E., Johnson M.P., Williams-Blangero S., Westra H.J., McRae A.F., Smith J.A., Kardia S.L., Hovatta I., Perola M., Ripatti S., Salomaa V., Henders A.K., Martin N.G., Smith A.K., Mehta D., Binder E.B., Nylocks K.M., Kennedy E.M., Klengel T., Ding J., Suchy-Dicey A.M., Enquobahrie D.A., Brody J., Rotter J.I., Chen Y.D., Houwing-Duistermaat J., Kloppenburg M., Slagboom P.E., Helmer Q., den Hollander W., Bean S., Raj T., Bakhshi N., Wang Q.P., Oyston L.J., Psaty B.M., Tracy R.P., Montgomery G.W., Turner S.T., Blangero J., Meulenbelt I., Ressler K.J., Yang J., Franke L., Kettunen J., Visscher P.M., Neely G.G., Korstanje R., Hanson R.L., Prokisch H., Ferrucci L., Esko T., Teumer A., van Meurs J.B., Johnson A.D. The transcriptional

- landscape of age in human peripheral blood. Nat Commun 2015; 6: 8570, https://doi.org/10.1038/ncomms9570.
- 44. Fleischer J.G., Schulte R., Tsai H.H., Tyagi S., Ibarra A., Shokhirev M.N., Huang L., Hetzer M.W., Navlakha S. Predicting age from the transcriptome of human dermal fibroblasts. Genome Biol 2018; 19(1): 221, https://doi. org/10.1186/s13059-018-1599-6.
- 45. Shokhirev M.N., Johnson A.A. Modeling the human aging transcriptome across tissues, health status, and sex. Aging Cell 2021; 20(1): e13280, https://doi.org/10.1111/ acel.13280.
- 46. Dimri G.P., Lee X., Basile G., Acosta M., Scott G., Roskelley C., Medrano E.E., Linskens M., Rubelj I., Pereira-Smith O. A biomarker that identifies senescent human cells in culture and in aging skin in vivo. Proc Natl Acad Sci U S A 1995; 92(20): 9363-9367, https://doi.org/10.1073/ pnas.92.20.9363.
- 47. Nadeau S., Cheng A., Colmegna I., Rodier F. Quantifying senescence-associated phenotypes primary multipotent mesenchymal stromal cell cultures. Methods Mol Biol 2019; 2045: 93-105, https://doi. org/10.1007/7651 2019 217.
- 48. Bruno S., Darzynkiewicz Z. Cell cycle dependent expression and stability of the nuclear protein detected by Ki-67 antibody in HL-60 cells. Cell Prolif 1992; 25(1): 31-40, https://doi.org/10.1111/j.1365-2184.1992.tb01435.x.
- 49. Kusumoto D., Seki T., Sawada H., Kunitomi A., Katsuki T., Kimura M., Ito S., Komuro J., Hashimoto H., Fukuda K., Yuasa S. Anti-senescent drug screening by deep learning-based morphology senescence scoring. Nat Commun 2021; 12(1): 257, https://doi.org/10.1038/s41467-020-20213-0.
- 50. Weber L., Lee B.S., Imboden S., Hsieh C.J., Lin N.Y.C. Phenotyping senescent mesenchymal stromal cells using AI image translation. Curr Res Biotechnol 2023; 5: 100120, https://doi.org/10.1016/j.crbiot.2023.100120.
- 51. Olova N., Simpson D.J., Marioni R.E., Chandra T. Partial reprogramming induces a steady decline in epigenetic age before loss of somatic identity. Aging Cell 2019; 18(1): e12877, https://doi.org/10.1111/acel.12877.
- **52.** Singh P.B., Laktionov P.P., Newman A.G. Deconstructing age reprogramming. Journal of Biosciences 2019; 44(4), https://doi.org/10.1007/s12038-019-9923-1.